Received: 26 November 2024 | Revised: 15 January 2025 | Accepted: 25 January 2025

DOI: 10.1002/alz.70012

Alzheimer's & Dementia®
THE JOURNAL OF THE ALZHEIMER'S ASSOCIATION

RESEARCH ARTICLE

Comparative mapping of single-cell transcriptomic landscapes in neurodegenerative diseases

E. Keats Shwab[1,2] | Zhaohui Man[1,2] | Daniel C. Gingerich[1,2] | Julia Gamache[1,2] | Melanie E. Garrett[3] | Geidy E. Serrano[4] | Thomas G. Beach[4] | Gregory E. Crawford[2,5,6] | Allison E. Ashley-Koch[3,7] | Ornit Chiba-Falek[1,2]

[1]Division of Translational Brain Sciences, Department of Neurology, Duke University Medical Center, Durham, North Carolina, USA

[2]Center for Genomic and Computational Biology, Duke University Medical Center, Durham, North Carolina, USA

[3]Duke Molecular Physiology Institute, Duke University Medical Center, Durham, North Carolina, USA

[4]Banner Sun Health Research Institute, Sun City, Arizona, USA

[5]Department of Pediatrics, Division of Medical Genetics, Duke University Medical Center, Durham, North Carolina, USA

[6]Center for Advanced Genomic Technologies, Duke University Medical Center, Durham, North Carolina, USA

[7]Department of Medicine, Duke University Medical Center, Durham, North Carolina, USA

Correspondence
Ornit Chiba-Falek, Division of Translational Brain Sciences, Department of Neurology, Duke University School of Medicine, Durham, NC 27710, USA.
Email: o.chibafalek@duke.edu

Funding information
National Institute of neurological disorders and stroke (NINDS)/NIH, Grant/Award Number: RF1-NS113548-01A1; National institute on aging (NIA)/NIH, Grant/Award Numbers: R01 AG057522, RF1 AG077695; Body Donation Program of Sun City

Abstract

INTRODUCTION: Alzheimer's disease (AD), dementia with Lewy bodies (DLB), and Parkinson's disease (PD) represent a spectrum of neurodegenerative diseases (NDDs). Here, we performed the first direct comparison of their transcriptomic landscapes.

METHODS: We profiled whole transcriptomes of NDD cortical tissue by single-nucleus RNA sequencing, using computational analyses to identify common and distinct differentially expressed genes (DEGs), pathways, vulnerable and disease-driver cell subtypes, and altered cell-to-cell interactions.

RESULTS: The same inhibitory neuron subtype was depleted in both AD and DLB. Potentially disease-driving neuronal cell subtypes were identified in both PD and DLB. Cell–cell communication was predicted to be increased in AD but decreased in DLB and PD. DEGs were most commonly shared across NDDs within inhibitory neuron subtypes. Overall, AD and PD showed greatest transcriptomic divergence, while DLB exhibited an intermediate signature.

DISCUSSION: These results may help explain the clinicopathological spectrum of these NDDs and provide unique insights into shared and distinct molecular mechanisms underlying pathogenesis.

KEYWORDS
Alzheimer's disease, cell communication, comparative, dementia with Lewy bodies, Parkinson's disease, single-nucleus RNA sequencing, synucleopathies, transcriptomics, vulnerable cell types

Highlights

- The same vulnerable inhibitory neuron subtype population was depleted in both Alzheimer's disease (AD) and dementia with Lewy bodies (DLB).

E. Keats Shwab and Zhaohui Man contributed equally to this study.

- Potentially disease-driving neuronal cell subtypes were discovered in both Parkinson's disease (PD) and DLB.
- Cell–cell communication was predicted to be increased in AD but decreased in DLB and PD.
- Differentially expressed genes were most commonly shared across neurodegenerative diseases in inhibitory neuron types.
- AD and PD had the greatest transcriptomic divergence, with DLB showing an intermediate signature.

1 | BACKGROUND

Age-associated neurodegenerative diseases (NDDs) such as Alzheimer's disease (AD), Parkinson's disease (PD), and dementia with Lewy bodies (DLB) exhibit overlapping clinical manifestations of molecular neuropathologies (Figure 1A). For example, Lewy bodies are present in more than half of AD cases,[1,2] and tau neurofibrillary tangles (NFTs) have been identified in brains of patients with familial PD (fPD).[3] Tau also appears to be a common component of Lewy bodies in association with α-Synuclein (*SNCA*).[4,5] Tau NFTs and amyloid beta (A*β*) plaques are also associated with DLB in ≈ 70% of cases,[6,7] indicating convergence of underlying pathological mechanisms of both AD and PD in DLB.[8] Evidence suggests that these co-pathologies of tau, A*β*, and *SNCA* aggregates are not merely coincidental but that these molecules are also likely involved in seeding the aggregation of one another.[9]

In addition to comorbidities and co-pathologies, shared genetic etiologies among these three NDDs were also reported. Genome-wide association studies (GWAS) focusing on each of these NDDs have identified variants separately associated with increased risk for AD,[10–12] PD,[13,14] and DLB,[15,16] and overlap in genetic risk factors between the NDDs has also been observed. For example, mutations in apolipoprotein E (*APOE*), the primary risk factor for AD, have also been linked to increased risk of DLB[15] and cognitive decline in PD.[17] Additionally, *SNCA* mutations have been similarly linked to both AD[18] and DLB[15] risk. Furthermore, mutations in GWAS AD risk genes, including *APP*,[19] *PSEN1*,[19–21] and *PSEN2*,[19,21] and GWAS PD risk genes, including *LRRK2*,[22] *MAPT*,[23] and *SCARB2*,[24] have also been experimentally linked to DLB. However, numerous loci with positive risk correlations for either AD or PD are not correlated with DLB risk.[15] These data indicate unique as well as common genetic underpinnings for each of these NDDs.

Most disease-associated single nucleotide variants (SNVs) are located in non-coding genomic regions, suggesting that in many cases allelic disease effects may derive from altered gene regulation rather than altered protein coding, and therefore, additional information is required to determine the relevant target genes impacted. The development of single-cell transcriptomics has helped elucidate these changes in gene regulation by enabling examination of expression patterns within individual brain cells of NDD patients at an unprecedented cell type and subtype resolution. This methodology has been applied individually to AD[25–28] and PD,[29,30] but for DLB only bulk transcriptomic studies have been previously performed.[31–33] Moreover, to our knowledge, no study to date has compared the transcriptional profiles across these NDDs. In this work, we used single-nucleus RNA sequencing (snRNA-seq) to directly compare for the first time the transcriptomic signatures of these three prevalent NDDs to elucidate shared and unique dysregulated genes and networks among these pathologies (Figure 1B). As the temporal lobe is commonly affected in the course of disease progression of each of the three NDDs,[34–38] we examined gene expression within temporal cortex (TC) samples to directly compare the transcriptomic landscapes across these pathologies. In addition to comparing each NDD to normal control (NC) samples, we also performed examinations of differential gene expression between each pair of NDDs (i.e., AD vs. PD, AD vs. DLB, PD vs. DLB), all at a granular cell subtype level of precision. We furthermore identified and characterized specific cell subtypes depleted in each of the NDDs, and predicted changes in cell-to-cell communication patterns associated with each disorder. Our findings yield novel insights into pathology-associated changes in gene expression that may facilitate the development of new detection and treatment strategies targeting specific NDDs or that may be potentially effective in the treatment of a range of disorders.

2 | METHODS

2.1 | Human *post mortem* brain tissue samples

The demographics, pathological notes, and other metadata for this study cohort are detailed in Table S1 in supporting information. Extensive pathology information for PD samples is provided in Table S2 in supporting information. Frozen human TC tissue samples from donors clinically diagnosed with AD ($n = 12$), DLB ($n = 12$), and NC donor samples ($n = 12$) were obtained from the Kathleen Price Bryan Brain Bank (KPBBB) at Duke University. Samples from donors diagnosed with PD ($n = 12$) were obtained from the Banner Sun Health Research Institute (BSHRI).[39] NCs were derived from donors with no clinical history of neurological disorder and samples had no neuropathological evidence of neurodegenerative diseases. Clinical diagnosis of AD was

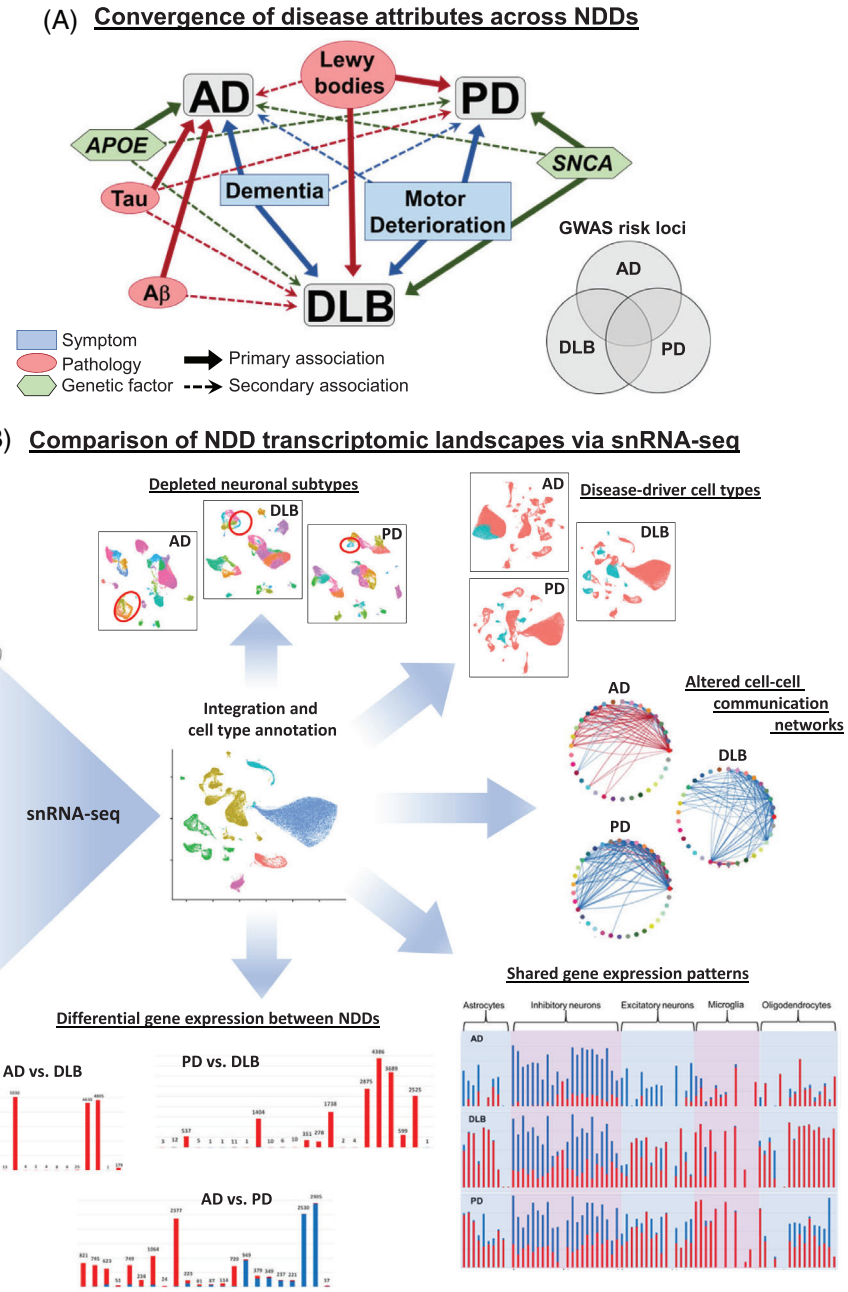

FIGURE 1 Elucidating similarities and differences in transcriptomic landscapes underlying shared and distinct pathologic attributes of AD, PD, and DLB. A, Convergence of disease attributes across NDDs. Dementia is a defining symptom of both AD and DLB but may also be present in PD, while motor deterioration is a primary symptom of PD and DLB but may also be present in AD. Lewy bodies are a hallmark of both PD and DLB, but are also present in more than half of AD cases, while tau and Aβ, hallmarks of AD, are often present in DLB, and tau is a common component of Lewy bodies. *APOE* variants represent the highest genetic risk factor for AD, but mutations have also been linked to DLB risk and cognitive decline in PD. *SNCA* is primarily associated with PD and DLB, but mutations in this gene are also are associated with increased risk of AD. Furthermore, numerous GWAS identified risk alleles show overlap across all three NDDs. B, Comparison of NDD transcriptomic landscapes via snRNA-seq. TC samples from 12 donors diagnosed with AD, DLB, and PD, as well as normal controls, were used for snRNA-seq analysis, followed by integration of transcriptomic datasets and cell type annotation. Datasets were examined for depletion of neuronal cell subtypes in each NDD compared to NC nuclei, identification of disease-driver cell types with enriched expression of GWAS genes, changes in cell-to-cell communication between cell subtypes in NDD and NC nuclei, shared genes differentially expressed in each NDD compared to NC nuclei, and differential gene expression between each pair of NDDs. Aβ, amyloid beta; AD, Alzheimer's disease; *APOE*, apolipoprotein E; DLB, dementia with Lewy bodies; GWAS, genome-wide association study; NC, normal control; NDD, neurodegenerative disease; PD, Parkinson's disease; snRNA-seq, single-nucleus RNA sequencing; TC, temporal cortex.

pathologically confirmed using Braak staging (AT8 immunostaining) and amyloid deposition assessment (4G8 immunostaining) for all AD samples. All AD tissue donors were in Braak & Braak stage III through V. DLB clinical diagnoses were pathologically confirmed based on criteria described by McKeith et al.[7] All DLB donors were confirmed to exhibit Lewy-related pathology within the neocortical, limbic, or brainstem regions and showed low levels of AD neuropathologic change (Braak stages I or II), with the exception of donor 1097 which exhibited Braak stage III pathology. Donor patient PD diagnoses were defined by the presence of two of the three cardinal clinical signs of resting tremor, muscular rigidity, and bradykinesia. Additionally, diagnoses of all PD samples were confirmed in autopsy by observation of pigmented neuron loss and the presence of Lewy bodies in the substantia nigra (SN). Neuropathological states of PD samples were confirmed *post mortem* using established clinical practice recommendations for McKeith scoring[40] and staging via the Unified Staging System for Lewy Body Disorders (USSLB).[41] All PD samples for which information was available had McKeith scores ranging from moderate to severe (2–4) in both the amygdala and SN. Where available, TC McKeith scores for most of the PD samples were either 0 or 1, with one sample each receiving scores of 2 and 3, indicating mild or absent PD pathology in this region for the majority of samples. USSLB stages of PD samples ranged from II to IV. PD samples 96–36 and 96–49 were lacking specific USSLB stage determination due to harvesting prior to BSHRI standardization of stage determination protocol. All tissue donors were White, with the *APOE* e3/e3 genotype. The project was approved for exemption by the Duke University Health System Institutional Review Board. The methods described were conducted in accordance with the relevant guidelines and regulations.

RESEARCH IN CONTEXT

1. **Systematic review**: The authors reviewed the literature using traditional sources (e.g., PubMed). While single-cell sequencing technology has been applied individually to Alzheimer's disease (AD) and Parkinson's disease (PD), for dementia with Lewy bodies (DLB), only bulk transcriptomic studies have been previously performed. Moreover, no study to date has compared the transcriptional profiles across these diseases. These relevant citations are appropriately cited.
2. **Interpretation**: Our findings are in alignment with the pathological phenotypes of the diseases, wherein AD and PD exhibit relatively distinct symptoms and molecular pathologies while DLB manifests clinical attributes of both conditions; the findings support a general view of a neuropathological continuum across the three diseases.
3. **Future directions**: These data contribute to a framework for future studies aimed at validating the contributions of the reported vulnerable and disease-driving cell types, dysregulated pathways, and cell–cell communication networks to diverse clinical outcomes in neurodegenerative diseases.

2.2 | Cohort statistics

For comparisons of demographic variables, R statistical programming language was used. Age and *post mortem* interval (PMI) of NC, AD, DLB, and PD diagnosis groups were compared (Table S3 in supporting information). The Shapiro–Wilk test was used to test for normal distribution of age and PMI values. As these were found unlikely to be normally distributed, Kruskal–Wallis *H* tests were used to determine significance of age and PMI differences between diagnosis group means.

2.3 | Nuclei isolation from *post mortem* human brain tissue

The nuclei isolation procedure has been described,[28] and was based on previous studies[42,43] and optimized for single-cell experiments. One hundred to 200 mg of human TC brain tissue samples were thawed in lysis buffer (0.32 M sucrose, 5 mM $CaCl_2$, 3 mM magnesium acetate, 0.1 mM ethylenediaminetetraacetic acid, 10 mM Tris-HCl pH 8, 1 mM dithiothreitol [DTT], 0.1% Triton X-100) and homogenized with a 7 mL dounce tissue homogenizer (Corning) and filtered through a 100 µm cell strainer, transferred to a 14 × 89 mm polypropylene ultracentrifuge tube, and underlain with sucrose solution (1.8 M sucrose, 3 mM magnesium acetate, 1 mM DTT, 10 mM Tris-HCl, pH 8). Nuclei were separated by ultracentrifugation for 15 minutes at 4°C at 107,000 g. Supernatant was aspirated, and nuclei were washed with 1 mL nuclei wash buffer (10 mM Tris-HCl pH 8, 10 mM NaCl, 3 mM $MgCl_2$, 0.1% Tween-20, 1% bovine serum albumin [BSA], 0.2 U/µL RNase inhibitor). Resuspended nuclei were centrifuged at 300 g New insights into the genetic etiology of Alzheimer's disease and related dementias for 5 minutes at 4°C, and supernatant was aspirated. Nuclei were then resuspended in wash and resuspension buffer (1X phosphate-buffered saline, 1% BSA, 0.2 U/µL RNase inhibitor), then filtered through a 35 µm strainer. Nuclei concentrations were determined using a Countess II Automated Cell Counter (ThermoFisher) and nuclei quality was assessed at 10X and 40X magnification using an Evos XL Core Cell Imager (ThermoFisher).

2.4 | snRNA-seq library preparation and sequencing

snRNA-seq libraries were constructed as described previously[28] using the Chromium Next GEM Single Cell 3′ GEM, Library, and Gel Bead v3.1 kit; Chip G Single Cell kit; and i7 Multiplex kit (10X Genomics) according to manufacturer's instructions. For each sample, 10,000 nuclei were targeted. Library quality control (QC) was performed on a Bioanalyzer (Agilent) with the High Sensitivity DNA Kit (Agilent) according to

manufacturer's instructions and the 10X Genomics protocols. Libraries were submitted to the Sequencing and Genomic Technologies Shared Resource at Duke University for quantification using the KAPA Library Quantification Kit for Illumina platforms and sequencing. Groups of four snRNA-seq libraries were pooled on a NovaSeq 6000 S1 50 bp PE full flow cell to target a sequencing depth of 400 million reads per sample (Read 1 = 28, i7 index = 8, and Read 2 = 91 cycles). Sequencing was performed blinded to age, sex, and diagnosis.

2.5 | snRNA-seq data processing

Raw snRNA-seq sequencing data were converted to FastQ format, aligned to a GRCh38 pre-mRNA reference, filtered, and counted using CellRanger 4.0.0 (10X Genomics). Subsequent processing was done using Seurat 4.0.1.[44] Filtered feature-barcode matrices were used to generate Seurat objects for the individual samples. For QC filtering, nuclei below the 1st and above the 99th percentile for number of features were excluded. Nuclei above the 95th percentile for mitochondrial gene transcript proportion (or > 5% mitochondrial transcripts if 95th percentile mitochondrial transcript proportion was < 5%) were also excluded. Because experiments were conducted in nuclei rather than whole cells, mitochondrial genes were subsequently removed. The individual sample Seurat objects were merged into one, and were iteratively normalized using SCTransform[45] with glmGamPoi, which alleviates bias from weakly expressed genes.[46] Batch correction was performed using reference-based integration[47] on the individual sample normalized datasets, which improves computational efficiency for integration.

2.6 | Doublet/multiplet detection in snRNA-seq data

Multiplets comprising different cell types (heterotypic) were excluded from snRNA-seq data by considering the "hybrid score," as described previously.[28] The hybrid score is calculated as $(x_1 - x_2) / x_1$, where x_1 is the highest and x_2 is the second highest prediction score.[48] Heterotypic multiplets would be expected to exhibit competing cell type prediction scores due to the presence of transcriptomic/epigenomic profiles from multiple cell types. Multiplets composed of one cell type (homotypic) were identified based on the number of features per cell. snRNA nuclei with feature counts > 99th percentile were excluded. Removal of homotypic multiplets in this manner is expected to also aid in filtering of heterotypic multiplets.

2.7 | Cell type and subtype cluster annotation

Cell type annotation was conducted using a label transfer method[47] and a previously annotated reference dataset from human M1. Batch-corrected data from both our dataset and the human M1 dataset were used for label transfer. Nuclei with maximum prediction scores of < 0.5 were excluded. Nuclei with a percent difference of < 20% between first and second highest cell type prediction scores were termed "hybrid" and excluded.[48] Endothelial cells and vascular leptomeningeal cells (VLMCs) were in low abundance and did not form distinct Uniform Manifold Approximation and Projection for Dimension Reduction (UMAP) clusters and were thus excluded. Proportion values of each cell type were tested for normal distribution using the Shapiro–Wilk normality test and found likely to be normally distributed. One-way analysis of variance (ANOVA) was used to test for group differences in mean cell type proportions between diagnosis groups for each major cell type. Two-tailed *t* tests were used to compare differences in mean cell type proportions between samples obtained from the BSHRI Brain and Body Donation Program (PD samples) and the Duke Alzheimer's Disease Research Center (ADRC) KPBBB (NC, AD, and DLB samples). ANOVA and *t* test *P* values for the six major cell types were then adjusted for multiple testing using the Benjamini–Hochberg false discovery rate (FDR) method. After principal component analysis (PCA), dimensionality was examined using an elbow plot and by calculating variance contribution of each principal component (PC). UMAP was then run using the first 30 PCs, and nuclei were clustered based on UMAP reduction. The resolution levels for cluster delineation were selected after comparison of a range of values as it was determined to provide optimal distinction between populations of nuclei displaying unique gene expression profiles as evidenced by their separation from one another in UMAP space. Counts of predicted major cell types based on the label transfer were examined for each of the clusters, and clusters were manually annotated based on the majority cell type for each cluster (e.g., "Exc1," "Exc2," etc.). Proportions of nuclei belonging to each cell type were calculated for each donor sample by dividing the number of nuclei annotated with a particular cell type by the total number of nuclei from that sample in the dataset. Where noted, clusters were also subsequently annotated using the scMayoMap[49] R package.

2.8 | Human M1 reference data processing

To optimize label transfer, we re-processed previously published human primary motor cortex (M1) snRNA-seq data[50] to map it to GRCh38 Ensembl 80 as we did with our data.[28] FastQ files were obtained from the Neuroscience Multi-omic Data Archive (NeMO: https://nemoarchive.org/) and were aligned to the same GRCh38 pre-mRNA reference used for our data, filtered, and counted using CellRanger 4.0.0 (10X Genomics). Filtered feature-barcode matrices were used to generate separate Seurat objects for each sample, with nuclei absent from the annotated metadata excluded. Seurat objects were merged and iteratively normalized using SCTransform[45] with glmGamPoi. Batch correction was performed using reference-based integration[47] on the normalized datasets. The 127 transcriptomic cell types in this data were grouped into eight broad cell types, including astrocytes, endothelial cells, excitatory neurons, inhibitory neurons, microglia, oligodendrocytes, oligodendrocyte precursor cells (OPCs), and VLMCs.

2.9 | Covariate selection for differential analyses

Prior to differential analysis, as previously described,[28] we estimated the impact of multiple technical variables as well as donor-level characteristics separately for the snRNA-seq experiments (Table S1). Read counts were summed for all nuclei in each donor sample, resulting in only one expression value per sample per gene, as all nuclei from a particular donor would have identical donor characteristics. Genes with no expression for > 20% of samples were subsequently removed, and all values were mean-centered and scaled prior to covariate analysis. PCA was then performed for genes using prcomp in R. We then carried out linear regression using glm in R for PCs explaining > 10% of the variability in global expression on both nuclei- and donor-specific metadata variables to identify factors that should be included as covariates in differential analyses. Specifically, we selected the variable most associated (surpassing Bonferroni correction for multiple testing, $q < 0.05$) with PC1 (or alternatively, the PC explaining the most variability) and regressed all genes on the associated variable to obtain gene residuals that are adjusted for its effect. We then performed PC analysis on the gene residuals, and in an iterative process, repeating the above steps until no additional metadata variables were associated with global expression ($q < 0.05$). After this process, age, sex, PMI, number of nuclei after QC filtering, median genes per cell, and average library size were selected as covariates for differential expression gene analysis.

2.10 | Cell-type proportion comparisons

To assess the selective loss of neuronal subtypes in each NDD, we performed a depletion analysis using a beta regression model implemented in the glmmTMB package in R. The proportion of each neuronal subtype within each sample was calculated, and the association between the proportion and disease status was examined while adjusting for potential confounding variables such as age, sex, PMI, and the number of nuclei after filtering. The significance of the depletion was determined based on the Benjamini–Hochberg (FDR) adjusted *P* values derived from the beta regression model.

2.11 | Marker gene identification

To identify genes differentially expressed between depleted neuronal subtypes in each disease condition, we used the FindMarkers function from the Seurat package. The analysis was performed using a likelihood-ratio test, adjusting for latent variables including age, sex, PMI, and the number of nuclei after filtering. The gene expression comparison was made between the depleted neuronal subtypes in the disease samples and their corresponding subtypes in the control samples. Genes with a Benjamini–Hochberg (FDR) adjusted *P* value < 0.05 were considered significantly differentially expressed. The differentially expressed genes (DEGs) were further categorized into upregulated and downregulated genes based on their average log2 fold change.

2.12 | Differential expression analysis

To identify DEGs at both the cell type and subtype levels between samples within our snRNA-seq dataset, we used the NEBULA algorithm.[51] Specifically, the NEBULA-HL method was used as this process is optimized for estimating both nucleus-level and donor-level data overdispersions.[51,52] Prior to running NEBULA, for each cell type and cluster, genes expressed in < 10% of cells in either group (PD or Normal) were filtered out. Age, sex, PMI, number of nuclei after QC filtering, median genes per cell, and average library size were included as fixed effects for NEBULA and sample donor ID was included as a random effect. Benjamini–Hochberg (FDR) correction for multiple testing was applied at the gene level to NEBULA-derived *P* values. Adjusted *P* values < 0.05 were deemed significant.

2.13 | Vulnerable cell type identification

For each broad cell type in each disorder, DEGs were identified using the NEBULA algorithm as described above. GWAS-associated genes for each disorder were obtained from published studies, considering genes located within 500 kilobases upstream or downstream of the GWAS single nucleotide polymorphism chromosome locus. To create gene sets representing the convergence of genetic risk factors and cell type–specific dysregulation, we intersected the GWAS-associated genes with the DEGs identified for each broad cell type in each disorder. The resulting gene sets were considered the putative driving forces or risk factors for the corresponding disorder. The vulnerability of each cell subtype to the disorder-specific gene sets was assessed using the AUCell package in R. For each cell subtype in each disorder, the following steps were performed:

1. The scRNA-seq data were subsetted to include only the cells belonging to the specific cell subtype.
2. The gene expression matrix was normalized and log-transformed.
3. The AUCell algorithm was applied to calculate the enrichment of the disorder-specific gene set in each cell, resulting in an area under the curve (AUC) score for each cell.
4. Cells were assigned to a "vulnerable" or "non-vulnerable" group based on the AUC score threshold determined using the AUCell_exploreThresholds function.

To identify marker genes associated with the vulnerable cell subtypes, differential gene expression analysis was performed using the FindMarkers function in Seurat. The analysis was conducted between the vulnerable and non-vulnerable cells within each cell subtype, controlling for potential confounding variables. Genes with an FDR-adjusted *P* value < 0.05 were considered significantly differentially expressed and were classified as marker genes.

2.14 | Differential cell-to-cell communication

To investigate the role of cell–cell communication in the progression of NDDs, we used CellChat, an R package for inference and analysis of intercellular communication networks from scRNA-seq data.[53] CellChat integrates scRNA-seq data with a curated database of ligand–receptor interactions to quantify communication probabilities between cell populations and identify significant interactions. For each disease–normal pair, we created separate CellChat objects using the normalized data matrix and cell type annotations. We then applied CellChat functions to identify overexpressed genes and interactions, compute communication probabilities, and filter interactions. The inferred communication networks were stored in the CellChat object. To visualize the differences in cell–cell communication between disease and normal conditions, we used CellChat's plotting functions.

2.15 | Biological pathway enrichment analysis

To understand the biological significance of gene sets derived from differential expression analyses, we used the Metascape[54] algorithm (https://www.metascape.org). The gene set of interest was input as the target gene list, and the total set of genes examined in the corresponding differential expression analysis was input as the background gene list. Gene Ontology (GO) terms were considered significantly enriched with a fold enrichment of at least 1.5 and an FDR-corrected enrichment P value < 0.01. To group the enriched Metascape output GO terms into broader biological categories, kappa similarities were determined for each pair of enriched GO terms, forming trees of hierarchical associations between terms, which were then used to delineate clusters of related terms. We then qualitatively assigned a major functional category label to each cluster based on assessment of common biological processes represented by the clustered GO terms.

2.16 | Genome version and coordinates

All genomic data and coordinates are based on the December 2013 version of the genome: hg38, GRCh38.

3 | RESULTS

3.1 | Annotation of cell types and subtypes in the human TC of individuals with AD, DLB, PD, and neurologically normal controls

Nuclei were isolated from frozen *post mortem* human TC tissues of 12 NC donor individuals with no NDD diagnosis or pathological signs, and 12 donors each with diagnoses and corresponding *post mortem* pathology of AD, DLB, and PD. Each diagnosis group comprised six females and six males (Table S1 summarizes the demographic and neuropathological phenotypes). snRNA-seq was carried out on prepared gene expression libraries. After QC filtering, expression data for nuclei from all four diagnosis groups were integrated, and data from 396,867 nuclei were retained across all four groups (Table S1). Nuclei were then annotated according to major brain cell types by label transfer[47] from a pre-annotated reference snRNA-seq dataset.[55] These included 19,962 astrocytes, 92,322 excitatory neurons, 44,807 inhibitory neurons, 25,926 microglia, 196,448 oligodendrocytes, and 17,402 OPCs. Other cell types including endothelial cells and vascular and leptomeningeal cells made up < 1% of the total cell population and were therefore excluded from the dataset in downstream analyses. Mean proportions of each cell type were found not to differ significantly among the four diagnosis groups (Figure S1A in supporting information), nor between samples obtained from the BSHRI and the Duke ADRC (Figure S1B). Overall, nuclei from individual donor samples of all diagnosis groups showed qualitatively similar distribution to one another across major cell types (Figure S2 in supporting information).

3.2 | Vulnerable neuronal types depleted in NDDs compared to neurologically normal controls

AD, DLB, and PD are characterized by the progressive loss of neurons in the brain. To characterize the specific neuronal types that are vulnerable in the TC of each pathology, we performed a comparison analysis of cell-type proportions for each NDD versus NCs, restricted to nuclei annotated as excitatory or inhibitory neuronal cells. Expression data for neuronal NC cells were separately integrated with neurons of each NDD. Integrated neuronal cells were then divided into numbered cell subtype clusters, with 30 neuronal subtype clusters for AD, 29 clusters for DLB, and 26 clusters for PD (Figure 2A). Examination of expression of markers for specific neurotransmitter types among neuronal cell types of each NDD showed the presence of only glutamatergic cell types among excitatory neuron clusters, and GABAergic cell types among inhibitory neuron clusters (Figure S3A in supporting information). We then performed a depletion analysis using a beta regression model and calculated the proportion of nuclei from a particular donor sample within each neuronal subtype cluster compared to the total neuronal nuclei for the same sample, and compared the proportions between NDD and NC donors. The results identified four vulnerable neuronal subtypes significantly depleted across the three NDDs (Figure 2A). Two of these were identified in AD, including one excitatory neuron subtype, AD-Exc7 (P_{adj} = 6.46e-5), and one inhibitory neuron subtype, AD-Inh10 (P_{adj} = 1.90e-5). In DLB, we identified one depleted inhibitory neuron subtype, DLB-Inh10 (P_{adj} = 1.65e-15), and in PD one depleted inhibitory neuron subtype, PD-Inh6 (P_{adj} = 8.53e-7). Of note, the analysis demonstrated that the same inhibitory neuron subtype is depleted in both AD and DLB.

To characterize the unique transcriptional patterns in the context of disease of each of these depleted subtypes compared to subtypes that were not depleted, we used a likelihood-ratio test to identify DEGs between each depleted cluster and the other clusters of the

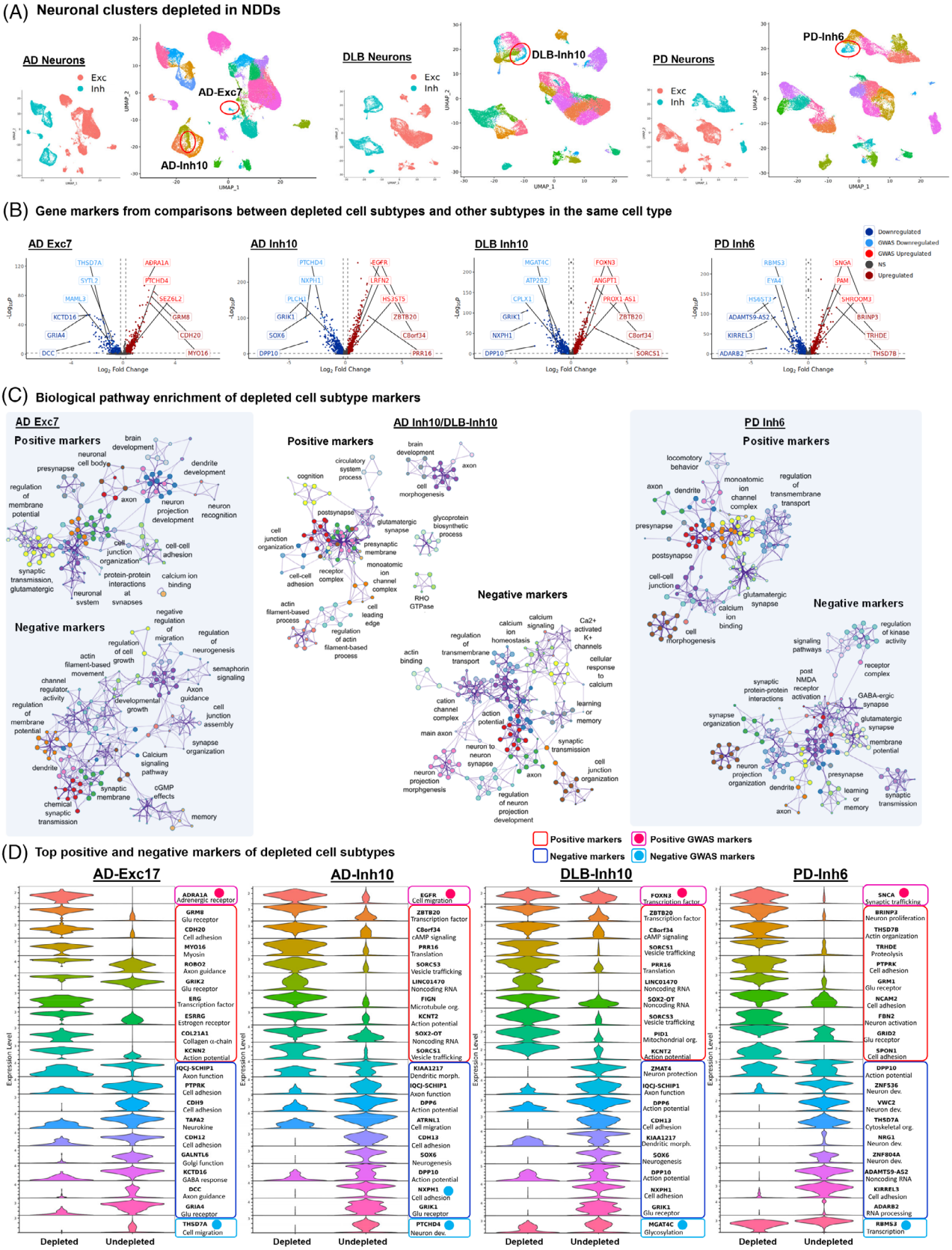

FIGURE 2 Characterization of vulnerable depleted cell subtypes in each NDD. A, Uniform Manifold Approximation and Projection for Dimension Reduction plots of neuronal nuclei of each NDD integrated with NC nuclei. Smaller plots are color coded to indicate excitatory neurons (Exc) and inhibitory neurons (Inh). Larger plots are color coded to indicate cell subtype clusters. Depleted clusters are circled in red and labeled. B, Unbiased volcano plots for depleted cell subtype clusters. Log2 fold change (FC) between depleted cluster nuclei and other nuclei of the same

same annotated cell type (i.e., excitatory or inhibitory neurons), adjusting for the latent variables age, sex, PMI, and the number of nuclei after filtering. The comparison was made between the depleted neuronal subtypes and non-depleted subtypes in the disease samples only. DEGs (FDR-adjusted *P* value < 0.05) were further categorized into positive (upregulated) and negative (downregulated) genes based on their average $\log_2$ fold change (Figure 2B, Tables S4–S7 in supporting information). Strikingly, comparison of positive and negative marker genes across all three depleted inhibitory neuron clusters revealed > 97% marker gene identity between clusters AD-Inh10 and DLB-Inh10. Furthermore, cell barcode comparison revealed that > 99% of the same NC neuronal cells were present in both clusters, strongly indicating that the two clusters represent the same neuronal subtype, depleted in both AD and DLB. Examination of expression of canonical inhibitory neuron markers used in previous studies[56–60] among inhibitory subtypes of all NDDs showed the depleted Inh clusters of AD and DLB to be distinguished from other subtypes by strong co-expression of *VIP*, *TAC3*, *PROX1*, *CNR1*, and *TSHZ2*, as well as low expression of *STXBP6*, *LHX6*, *CUX2*, and *PHACTR2*, among other marker genes (Figure S3B). In contrast, no cell type with a comparable canonical marker expression signature was identified among PD inhibitory neuron clusters.

To better understand the biological significance of differential gene expression in the vulnerable neuronal clusters, we examined enrichment of particular biological pathways among positive and negative markers of each depleted subtype,[54] and generated networks of enriched pathways grouped by shared gene membership (Figure 2C). For all depleted clusters, we primarily found common DEGs associated with functional categories relating to neuronal development and organization (e.g., neuron projection development, axon guidance), synaptic structure (e.g., presynapse, postsynapse, cell–cell adhesion), and synaptic transmission (e.g., regulation of membrane potential, monoatomic ion channel complex, synaptic protein–protein interactions), suggesting that nuances of neuron organization and synaptic function play an important role in determining susceptibility to neurodegeneration.

Examining specific positive and negative marker genes with the most strongly altered (largest fold-change) gene expression in vulnerable neuronal subtypes (Figure 2D), we found that in AD-Exc7, glutamate receptor-encoding genes *GRM8* and *GRIK2* were among the most strongly upregulated, while the glutamate receptor gene *GRIA4* was among the most strongly downregulated. The cadherin-encoding gene *CDH20*, regulating cell–cell adhesion, was also strongly upregulated, while the cadherin genes *CDH9* and *CDH12* were downregulated, as was *PTPRK*, also involved in cell adhesion. To identify marker genes more likely to be involved in driving NDD pathology, we defined genes proximal (within 500Kb) to GWAS-identified risk loci for a particular NDD as "GWAS genes." Based on GWAS-identified risk loci for AD,[10,11] the adrenergic receptor gene *ADR1A* was the most strongly upregulated AD-GWAS gene marker for AD-Exc7, while the cell migration regulatory gene *THSD7A* was the most strongly downregulated AD-GWAS gene marker.

As noted, depleted subtypes AD-Inh10 and DLB-Inh10 largely shared the same marker genes. The strongest positive markers for both these types included the transcription factor (TF) gene *ZBTB20*, translational regulator *PRR16*, and *SORCS1* and *SORCS3*, both involved in vesicle trafficking and likely playing a role in synaptic transmission. The most strongly upregulated AD-GWAS gene marker was *EGFR*, involved in cell migration, while the most strongly downregulated AD-GWAS gene marker was *PTCHD4*, involved in neuronal development. Based on GWAS-identified risk loci for DLB,[15,16] the most strongly upregulated DLB-GWAS gene marker was the TF-encoding *FOXN3*, while the most strongly downregulated DLB-GWAS gene was *MGAT4C*, involved in protein glycosylation.

The subtype depleted in PD, PD-Inh6, showed marked upregulation of glutamate receptor genes *GRM1* and *GRID2*, as well as cell adhesion–regulating genes *NCAM2* and *SPON1*, while downregulation of several developmental genes was observed, including *ZNF536*, *VWC2*, *NRG1*, and *ZNF804A*. Notably, the most strongly upregulated PD-GWAS gene marker (based on GWAS-identified risk loci for PD[13]) for this cluster was *SNCA*, suggesting that overexpression of the *SNCA* gene correlates with vulnerability to neurodegeneration in PD. The most strongly downregulated PD-GWAS gene marker was the transcriptional regulatory gene *RBMS3*.

major cell type is plotted against −log10 *P* value (FDR). Points representing DEGs with statistically significant (FDR < 0.05) upregulation in NDD are shown in dark red while DEGs with significant downregulation are shown in dark blue. Genes without significantly differential expression are shown as gray points. The three DEGs with the highest absolute fold change (log2FC > 0.2) in the up- and downregulated categories are labeled in dark red and dark blue, respectively. The three DEGs within 500 kb of NDD-associated single nucleotide polymorphisms previously identified in GWAS (GWAS-DEG) with the highest absolute log2FC in the up- and downregulated categories are labeled in bright red and bright blue, respectively. C, Metascape network plots of biological pathways enriched among genes upregulated (positive markers) and downregulated (negative markers) within depleted cell subtypes compared to cell subtypes of the same major cell type that were not depleted. Nodes represent specific biological pathways clustered by shared gene membership. Clusters with similar biological function are color coded and labeled according to general function. Node sizes are proportional to the number of differential-interacting genes in the pathway, and line width connecting nodes is proportional to shared gene membership in linked pathways. D, Violin plots of log-normalized count data showing expression of the GWAS-DEGs (bordered in pink and light blue) and 9 overall DEGs (bordered in red and dark blue) with the highest absolute fold change in depleted clusters compared to clusters of the same major cell type that were not depleted. Basic functional category information is indicated for each gene. AD, Alzheimer's disease; DEG, differentially expressed gene; DLB, dementia with Lewy bodies; FDR, false discovery rate; GWAS, genome-wide association study; NC, normal control; NDD, neurodegenerative disease; PD, Parkinson's disease.

3.3 | Characterization of disease-driver cell subtypes with enriched expression of GWAS-identified risk genes

We sought to identify cell subtypes that were potentially important for conferring risk of each NDD, hereafter disease-driver cell types, based on increased expression of GWAS genes. First, we integrated, annotated, and clustered nuclei of each NDD with NC nuclei as described above, except that in this case nuclei of all cell types, including astrocytes (Astro), excitatory neurons (Exc), inhibitory neurons (Inh), microglia (Micro), oligodendrocytes (Oligo), and OPCs were included rather than neuronal nuclei alone. This resulted in delineation of 32 cell subtype clusters in AD, 32 clusters in DLB, and 35 clusters in PD (Figure 3A). We next examined each subtype for enriched expression of GWAS genes using AUCell.[61] This program compares expression of a defined gene set (i.e., GWAS proximate genes) to total genes expressed in each nucleus, and determines whether the gene set is expressed in a significantly higher proportion than would be expected by chance. We defined a cluster as a disease driver if > 99% of nuclei showed significant enrichment for GWAS gene set expression. In this way, we identified one disease-driver oligodendrocyte cluster in AD (AD-Oligo3), four disease-driver excitatory neuron clusters (DLB-Exc1, 5, 8, 10) and two inhibitory neuron clusters (DLB-Inh1, 2) in DLB, and four disease-driver excitatory neuron clusters in PD (PD-Exc4, 5, 6, 7; Figure 3A, B). Thus, both DLB and PD produced multiple neuronal cell types that were implicated as disease drivers, while in AD only a single oligodendrocyte disease-driver cell subtype was identified.

To understand the potential functional significance of risk genes expressed in these disease-driver clusters, we performed marker gene analysis as above, comparing gene expression in disease-driver clusters of a particular cell type to all of the other clusters of that same cell type in NDD nuclei (Tables S8–S11 in supporting information). We then examined biological pathway enrichment among GWAS genes upregulated in each set of disease-driver cell types. Finally, we clustered enriched pathways based on common gene membership (Figure 3C). In the disease-driver oligodendrocyte cluster of AD, AD-Oligo3, we found enrichment of numerous pathways relating to endosomal vesicle trafficking (specific strongly upregulated genes relating to this pathway, including *SORL1*, *MYO1E*, and *PACS2* [Figure 3D]), cytoskeletal organization (e.g., *HYDIN*, *TANC2*, *STRN*), and regulation of proteolysis (e.g., *ADAMTS4*) and apoptosis (e.g., *DAPK2*, *TNFRSF21*). Notably, we also observed strongly inhibited expression of the major AD risk factor gene *BIN1* in this cell type (Table S8). In disease-driver excitatory neuron clusters of DLB, we identified enrichment of pathways relating to synaptic organization and transmission (e.g., *KCNN3*, *SLC29A4*, *C1QL2*), cell adhesion (e.g., *PCDH8*), transmembrane transport (e.g., *SLC2A12*, *MSFD4A*, *ATP7B*), DNA damage response (e.g., *CDC14B*), and proteolysis. Among disease-driver inhibitory neurons in DLB, we found enrichment of pathways relating to synaptic transmission (e.g., *ATP2B2*, *CPLX1*, *KCNC1*, *SCTR*), autophagy, proteolysis (e.g., *UBE3A*), and DNA damage response (e.g., *CDC148*, *FBXO31*). In disease-driver excitatory neurons of PD, we found enrichment of risk genes involved in synaptic organization and transmission (e.g., *SNCA*, *CAMK2D*, *RIMS1*, *SH3GL2*, *TMEM163*, *SYT17*, *KCNK10*), autophagy, phospholipid metabolism, and homologous recombination. It is notable that as for the PD-depleted neuron cluster above, *SNCA* was also among the top upregulated GWAS genes within PD-disease driver neuron clusters.

3.4 | Altered cell-to-cell communication pathways in NDDs

Next, we aimed to investigate changes in interactions between different cellular subtypes associated with each of the three NDDs. To accomplish this, we used the same integrated datasets of NC nuclei and nuclei of each NDD used above for analysis of disease-driver subtypes. We analyzed expression of known interacting ligands and receptors in each of the subtype clusters to identify pairs of subtypes with likely communication using CellChat.[53] Predicted interactions were then compared between NC and NDD nuclei to identify disease-associated changes in cell–cell communication. Comparisons were made regarding relative strength of interactions between cell subtypes based on changes in gene expression levels between NC and NDD nuclei of the same subtype.

Changes in interaction strength were varied across the three NDDs (Figure 4A, Figure S4 in supporting information). In AD, such changes were overall split between increased and decreased communication among different cell types, with both large increases and decreases observed among the top 10% of altered cell type interactions. The cell types with the largest increases in interaction strength included several excitatory neuron subtypes, AD-Exc1, 3, and 4, and inhibitory neuron subtype AD-Inh1, as well as oligodendrocyte subtypes AD-Oligo1 and 4. All these cell types showed primarily increased communication with neuronal subtypes. In contrast, decreased interaction strength was observed in astrocyte cluster AD-Astro1, excitatory neuron cluster AD-Exc2, and OPC cluster AD-OPC1, all of which showed reduced communication with one another as well as with several neuronal and oligodendrocyte subtypes. In DLB, by contrast, overall changes primarily showed decreases in interaction strength. Among the strongest effects, subtypes DLB-Astro1; DLB-Exc1, 3, 5, and 6; DLB-Inh1, 2, 3, and 4; DLB-Oligo1 and 5; and DLB-OPC1 showed reduced communication strength mainly with one another. However, subtypes DLB-Oligo1, 2, 3, 4, and 6 showed increased communication with one another as well. In PD, overall decreased interaction strength was also observed, with the strongest decreases found between the cell types PD-Astro1 and 2; PD-Exc1, 2, 3, 5, and 6; PD-Inh2 and 4; PD-Oligo1; and PD-OPC1. Increased interaction strength in PD was observed for clusters PD-Oligo2 and 4, primarily regarding other oligodendrocyte clusters. Overall, the results demonstrated increased interaction strength in AD driven primarily by excitatory neurons and oligodendrocytes, but decreased interaction strength in DLB and PD, driven primarily by both inhibitory and excitatory neurons, as well as oligodendrocytes. Thus, changes in cell–cell communication strength in DLB

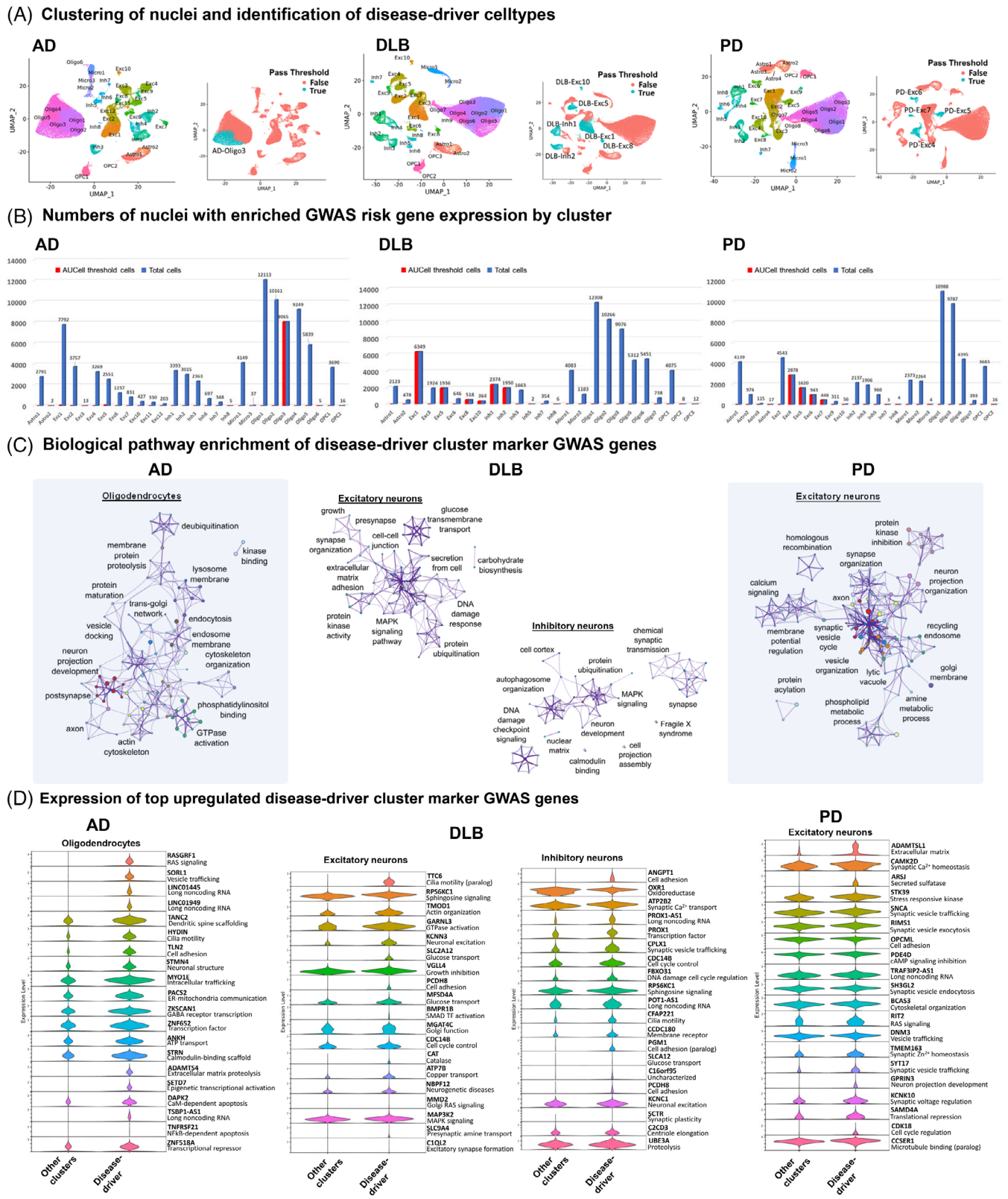

FIGURE 3 Identification of disease-driver cell subtypes with enriched GWAS risk gene expression. A, Uniform Manifold Approximation and Projection for Dimension Reduction plots of neuronal nuclei of each NDD integrated with NC nuclei. Smaller plots are color coded to indicate subtypes below (False) and above (True) the AUCell pass threshold for enriched expression of genes within 500 kb of NDD-associated single nucleotide polymorphisms previously identified in GWAS (GWAS genes). B, Bar charts showing total numbers of cells in each subtype cluster (blue) and numbers of cells above the AUCell pass threshold for enriched GWAS gene expression (red). C, Metascape network plots of biological

and PD closely resembled one another, while patterns in AD were more distinct.

To get new insights into the biological significance of cell–cell communication in the three NDDs, we examined the biological pathway associations of the genes involved in altered communication between each pair of cell subtypes using Metascape. Pathways enriched among genes associated with the top AD-increased interactions related primarily to cell growth, development, and morphology, as well as DNA damage response, stress response, and G protein-coupled receptor (GPCR) and kinase signaling (Figure 4Bi). The pathways enriched among AD-increased interactions across all cell types notably differed between neuron-to-neuron interactions and oligodendrocyte-to-neuron interactions (Figure 4Bii). Pathways strongly enriched among all interaction types were associated with cell growth and morphogenesis, and GPCR and tyrosine kinase receptor signaling, while interactions more strongly enriched in neuron-to-neuron interactions related specifically to nerve morphogenesis and organization, including axon guidance, nerve development, semaphorin signaling, and neurotrophin signaling.

In DLB, interaction strength was overall reduced compared to NC nuclei, and pathways enriched among genes associated with the top DLB-decreased interactions related primarily to cell growth and development, immune response signaling, and calcium homeostasis (Figure 4Ci). Pathway enrichment was strongest in DLB-decreased communications involving the Exc1 and Exc3 excitatory neuron subtypes as the transmitting cell type, with a wide variety of receiving cell types (Figure 4Cii). Pathways enriched specifically in these types of interactions related to cell growth and proliferation, cell morphogenesis, and the oxidative stress response. Pathways enriched among all interacting cell types additionally included calcium ion homeostasis, immune response signaling, chemotaxis, proteolysis, and general kinase signaling.

In PD, interaction strength was also reduced overall. Pathways enriched among genes associated with the top PD-decreased interactions again related to cell growth and development, and to axon guidance and neuronal organization, synaptic membrane structure, and regulation of apoptosis (Figure 4Di). Some specific pathways were most often enriched in PD-decreased communications in which neuronal subtypes were the transmitting cell type, including PI3K/AKT growth signaling, cyclic adenosine monophosphate signaling, and endocrine hormone signaling (Figure 4Dii). Many pathways involved in growth and development were enriched across all interaction types, as were pathways associated with regulation of apoptosis, cell adhesion, synaptic membrane organization, and enzyme-linked receptor signaling.

Next, to organize altered cell-to-cell communication networks with regard to the specific cell types involved, individual pairs of interacting proteins in NDD and NC nuclei were grouped by association with particular biological pathways, and each of these pathway groups were further clustered based on the particular cell subtypes in communication, after PCA (Figure S5A in supporting information). This led to the identification of four communication clusters each in AD and DLB, and five clusters in PD. In AD and PD; each cluster contained a qualitatively even distribution of pathways from both NC and NDD nuclei. However, in DLB, cluster 1 was entirely composed of communication pathways identified in NC nuclei, while cluster 3 was heavily dominated by pathways identified in DLB nuclei, suggesting the development of distinct cell-to-cell communication networks in the context of DLB (Figure S5B).

3.5 | Shared patterns of differential gene expression among NDDs

To identify commonalities in gene dysregulation among NDDs, we integrated snRNA-seq data from nuclei of all three NDDs and NC nuclei for each of the six major cell types and grouped these into cell subtype clusters as described above. Next, we further annotated these clusters as more specific predicted cell types using the scMayoMap[49] software package (Figure 5A), and used the NEBULA[51] software package to perform differential gene expression analysis between NC nuclei and those of each NDD at the cell subtype level. Across all three NDDs, the highest numbers of DEGs were identified in inhibitory neuron subtypes, and the majority were downregulated (Figure 5B). Most excitatory neuron and astrocyte clusters in AD exhibited primary gene downregulation, while, in DLB and PD both upregulated and downregulated DEGs were detected in those clusters. On the other side, microglia showed mixed up- and downregulation in AD, but predominantly upregulation in DLB and PD in most subtypes. OPC subtypes showed both up- and downregulation DEGs within each NDD. Oligodendrocytes were also varied, with mixed distribution of up- and downregulation in AD, predominant upregulation in DLB, and predominant downregulation in PD. Notably, *SNCA* was upregulated in DLB in four separate oligodendrocyte clusters (Oligo1, 3, 5, and 10), but not in oligodendrocyte clusters of PD, suggesting a potentially important function in

pathways enriched among GWAS genes upregulated within disease-driver cell subtypes compared to cell subtypes of the same major cell type that were not enriched for GWAS gene expression. Nodes represent specific biological pathways clustered by shared gene membership. Clusters with similar biological function are color coded and labeled according to general function. Node sizes are proportional to the number of differential-interacting genes in the pathway, and line width connecting nodes is proportional to shared gene membership in linked pathways. D, Violin plots of log-normalized count data showing expression of the GWAS-DEGs with the highest positive fold change in disease-driver clusters compared to clusters of the same major cell type that were not disease-driving. Basic functional category information is indicated for each gene. AD, Alzheimer's disease; DEG, differentially expressed gene; DLB, dementia with Lewy bodies; FDR, false discovery rate; GWAS, genome-wide association study; NC, normal control; NDD, neurodegenerative disease; PD, Parkinson's disease.

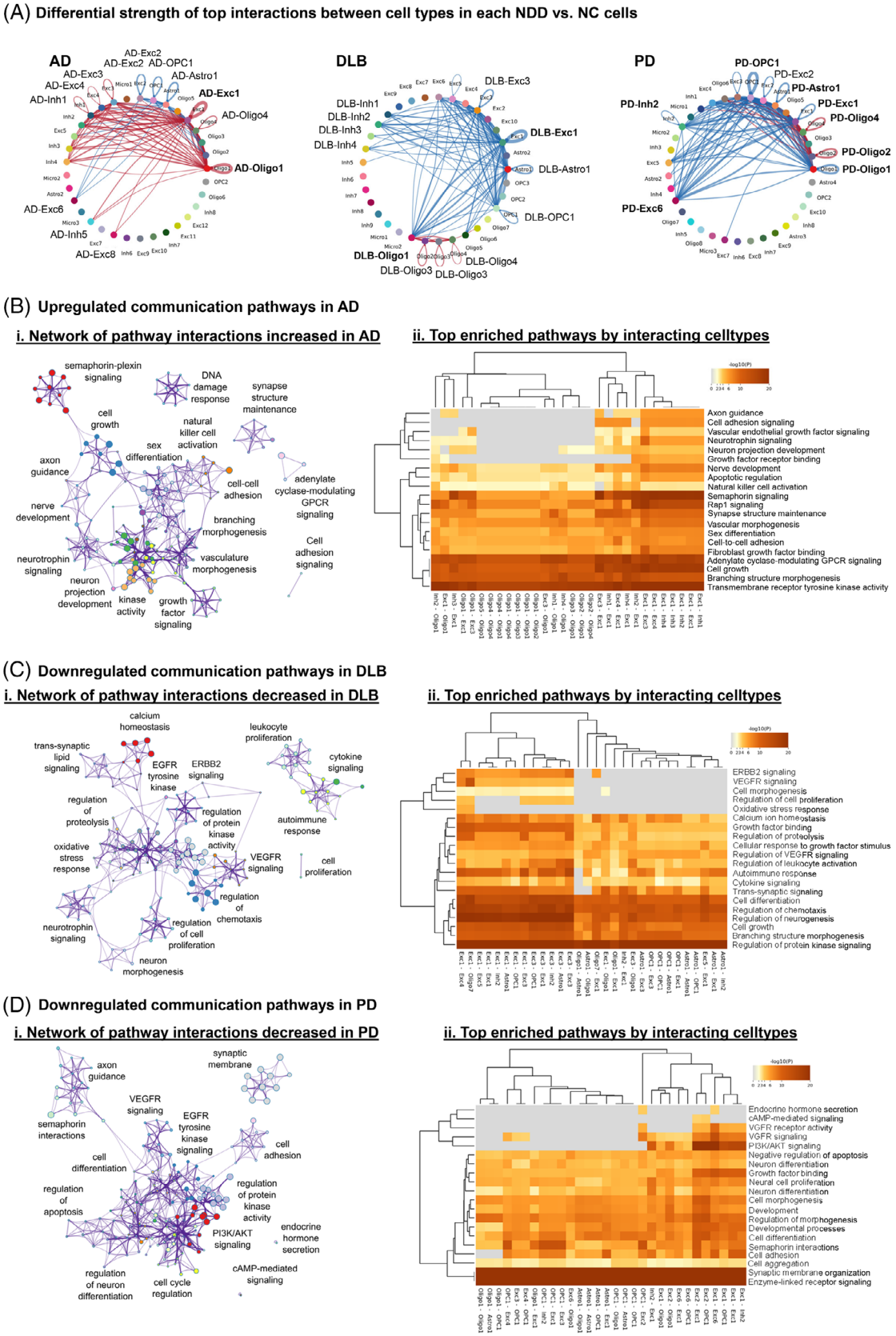

FIGURE 4 Differential interaction strength between cell subtypes in NDDs versus normal nuclei. Ai, CellChat heatmaps showing degree of overall change in interaction strength between all pairs of cell subtypes for each NDD. Red indicates increased interaction in NDD, blue indicates decreased interaction. Aii, CellChat network diagram showing cell types with the highest differential interaction strength based on fold change in receptor-ligand expression in NDD nuclei compared to NC. Lines between cell types indicate significantly altered interaction, with red lines

oligodendrocytes for this key synucleopathy gene specifically in the context of DLB.

Next, for each cell subtype, we catalogued the shared up- and downregulated DEGs across all three NDDs (Figure 5C). As expected, inhibitory neuron subtypes exhibited the highest number of DEGs and almost all were downregulated. The Interneuron 2 inhibitory neuron subtype exhibited the highest number of shared downregulated DEGs (5570; Figure 5D, Table S12 in supporting information), followed by the GABAergic neuron 1 subtype (3898; Figure 5E, Table S13 in supporting information). Additionally, ≈ 900 downregulated DEGs were shared between each pair of pathologies in Interneuron 2 (984 for AD and PD, 941 for AD and DLB, 876 for DLB and PD; Figure 5Di). Similarly, GABAergic neuron 1 also exhibited additional shared DEGs between each pair of NDDs (4713 for AD and PD, 423 for AD and DLB, 102 for DLB and PD; Figure 5Ei). Micro 10 had the highest number of shared upregulated DEGs (248; Figure 5F, Table S14 in supporting information). Examination of overlap between each pair of pathologies in Micro 10 identified the largest number of shared upregulated DEGs (476) between DLB and PD, and fewer shared DEGs between the other pairs (48 for AD and DLB, 33 for AD and PD; Figure 5Fi). In contrast, other major cell types shared only a relatively small number of DEGs. Overall, these results suggested that the common dysregulated pathways across NDDs are mainly found in inhibitory neurons.

Thus, we next analyzed the enrichment of biological pathways among shared downregulated DEGs in the Interneuron 2 and GABAergic neuron 1 subtypes. As these are pathways enriched among downregulated DEGs, they may reflect impaired biological pathways. In the Interneuron 2 subtype, we identified enrichment of pathways related to synaptic vesicle transport, mitochondrial function, oxidative phosphorylation, autophagy, proteolysis, and RNA processing (Figure 5Dii). These functional categories were also identified in the analysis of the top enriched individual pathways (Figure 5Diii). Specific genes that were strongly downregulated in all three NDDs included the TF gene *ETV5*, associated with the response to oxidative stress and the cell growth regulator gene *NELL1*, as well as the AD-GWAS gene *CBLN4*, involved in synapse organization; the DLB- and PD-GWAS gene *DPM3*, involved in endoplasmic reticulum (ER) function; and the autophagy-associated PD-GWAS gene *RNASEK* (Figure 5Div). The respective DLB- and PD-GWAS genes *NEK5* and *TIMP2*, both involved in regulation of proteolysis, were strongly downregulated in both DLB and PD.

In the GABAergic neuron 1 subtype, the identified enriched pathways based on shared downregulated DEGs were overall similar to those of Interneuron 2 (Figure 5Eii), including aerobic respiration and respiratory electron transport, translation, metabolism of RNA, and mitochondrion organization (Figure 5Eiii). *ETV5* and *DPM3* were again among the most highly downregulated genes in all three NDDs, as was the AD-GWAS gene *VGF*, involved in regulation of neuroplasticity, and the AD- and PD-GWAS GABA-receptor interacting gene *GABARAP* (Figure 5Eiv). Developmental regulator *WNT3*, a GWAS gene for both AD and PD, was also highly downregulated in those two NDDs.

Similarly, we analyzed pathway enrichment in upregulated DEGs of the Micro10 subtype, plausibly indicating activation of biological pathways. The results demonstrated enrichment for growth and developmental pathways, as well as pathways associated with leukocyte activation, cell cycle regulation, DNA damage response, chromatin organization, and cytoskeletal organization (Figure 5Fii). The strongest enriched individual pathways included chromatin organization, growth factor signal transduction, receptor tyrosine kinase signaling, and NOTCH1 signaling (Figure 5Fiii). The TF genes *ELF2* and *MAML3*, and the deubiquitinase gene *USP3*, all AD-GWAS genes, and the transcriptional regulator PD-GWAS gene *LCORL* were among the most strongly overexpressed DEGs across all three NDDs, as were the actin motor gene *MYO9B*, and the cell growth signaling gene *PTPRC* (Figure 4Fiv). The gene *DOCK2*, involved in chemokine-responsive cytokinesis, was strongly upregulated in both AD and DLB, while the DLB-GWAS gene *SLCO2B1*, also involved in cell growth signaling; the steroid transport gene *CYB5R4*; the PD-GWAS gene *DISC1*, regulating neuronal development; and the ER monooxygenase gene *TBXAS1*, were strongly upregulated in both PD and DLB. In summary, we observed high numbers of shared downregulated genes in inhibitory neuron subtypes across all three NDDs, indicating impairment of pathways relating to neuronal development, synaptic function, stress responses, and other categories, but more diverse expression patterns in other types, with fewer shared DEGs.

3.6 | Differential gene expression between NDDs

To advance the understanding of mechanistic diversity among NDDs, we next studied the differential transcriptomic landscape between

indicating increased interaction strength in NDD and blue lines representing decreased interaction strength. Line width is proportional to statistical significance of change in interaction strength. Larger and bold labels indicate cell types with more prominently altered interactions. Bi, Metascape network plot of biological pathways enriched among genes associated with increased interaction strength in AD across all cell types. Nodes represent specific biological pathways clustered by shared gene membership. Clusters with similar biological function are color coded and labeled according to general function. Node sizes are proportional to the number of differential-interacting genes in the pathway, and line width connecting nodes is proportional to shared gene membership in linked pathways. Bii, Heatmap of top 20 enriched pathways among interactions increased in AD across all cell types. Interacting cell types are indicated, with sending type listed first and receiving type indicated second. Color saturation is proportional to strength of enrichment. Ci, Metascape network plot of biological pathways enriched among genes associated with increased interaction strength in DLB across all cell types. Cii, Heatmap of top 20 enriched pathways among interactions increased in DLB across all cell types. Di, Metascape network plot of biological pathways enriched among genes associated with increased interaction strength in PD across all cell types. Dii, Heatmap of top 20 enriched pathways among interactions increased in PD across all cell types. AD, Alzheimer's disease; DLB, dementia with Lewy bodies; GWAS, genome-wide association study; NC, normal control; NDD, neurodegenerative disease; PD, Parkinson's disease.

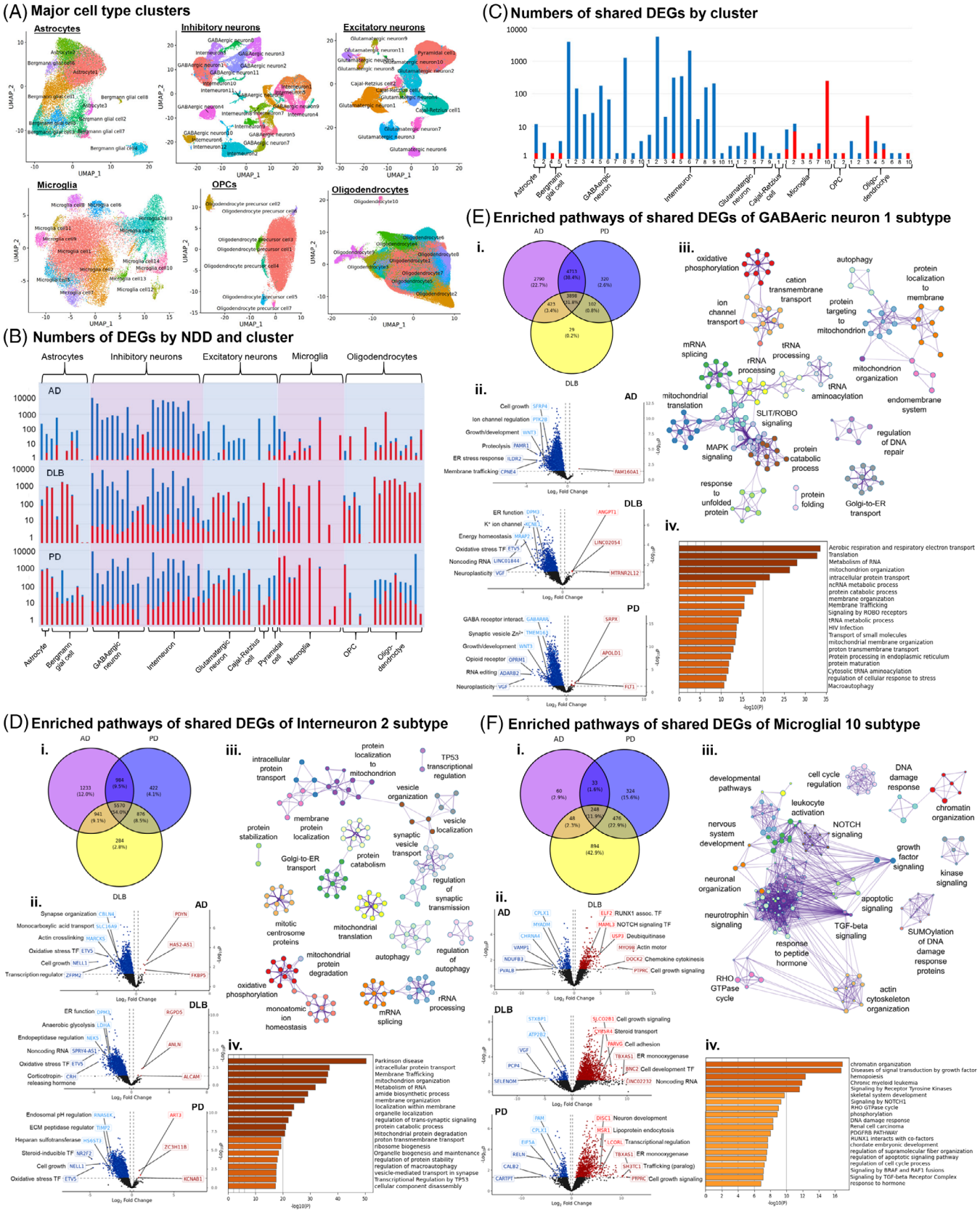

FIGURE 5 Differential gene expression shared by three pathologies on cell subtype level. A, Uniform Manifold Approximation and Projection for Dimension Reduction plots of integrated NDD and NC nuclei of each major cell type, color coded to indicate cell subtype clusters. B, Bar charts representing numbers of DEGs identified in each cell subtype within each NDD compared to NC nuclei of the same subtype. Red indicates DEGs upregulated in NDDs and blue indicates DEGs downregulated in NDDs. C, Bar chart representing numbers of DEGs shared between all three NDDs compared to NC nuclei for each cell subtype. Red indicates DEGs upregulated in NDDs and blue indicates DEGs downregulated in NDDs.

NDDs. To accomplish this, we integrated transcriptomic data for all cell types from each pair of NDDs (i.e., AD and DLB, PD and DLB, and AD and PD) and performed dimensional reduction and clustering of the integrated datasets to identify cell subtypes (Figure 6A). Differential expression analysis was performed at the cell subtype level for each NDD pairing to identify distinct DEGs between the pathologies. Comparing AD and DLB, we found DEGs that were upregulated in DLB in only 4 out of the 29 cell subtype clusters, including excitatory neurons (clusters 5 and 9), and oligodendrocytes (clusters 1 and 2), which exhibited ≈ 5000 DEGs each (5347, 5030, 4630, and 4805, respectively), mainly upregulated in DLB (Figure 6B, Ci, Tables S15–S18 in supporting information). The only other clusters that exhibited > 100 DEGs were Exc3 and Oligo6. Biological pathway enrichment analysis of DLB-upregulated DEGs in the excitatory neuron subtypes revealed enrichment of genes involved in cell cycle regulation, synaptic transmission, and stress response. In oligodendrocyte clusters, we found enrichment for pathways associated with inclusion body assembly, cellular signaling, and chromatin organization (Figure 6Cii). In addition, genes involved in DNA damage response, proteolysis, immune response, and transcriptional regulation were enriched in both these cell types. Accordingly, the strongest DLB-upregulated genes also play roles in these functional categories, including GWAS risk genes for both AD and DLB (Figure 6Ci). For example, *RTF2*, a DEG in Exc5 and Oligo2, and *FBXO31* in Oligo2 are involved in DNA damage response, and the DEGs *SUGT1* in Exc5, *CCNE2* in Exc9, and *GAK* in Oligo1 and 2, among others, are involved in cell cycle regulation. The proteolysis associated gene *MAEA* is a GWAS risk gene for both AD and DLB and was among the highest DLB-upregulated DEG in both Exc9 and Oligo1. The growth factor signaling AD-GWAS gene *PLCG2* was highly DLB-upregulated in all four cell types.

Comparison of PD to DLB across all clusters also resulted mainly in DLB-upregulated DEGs (Figure 6B, Di, Tables S19–S22 in supporting information). Genes were strongly upregulated in DLB in a number of oligodendrocyte clusters (2875, 4386, 3689, and 2525 in Oligo1, 2, 3, and 5, respectively), with fewer DEGs in excitatory neuron clusters (537 and 1404 in Exc1 and 4, respectively). Additionally, while the Micro2 cluster was annotated as a microglial cluster due to this being the most prevalent cell type, excitatory neuron nuclei comprised approximately one third of the cluster and > 10% of the cluster was made up of oligodendrocyte cells. For this reason, we separately performed differential expression analysis on each of these three cell types within the cluster. We identified 6.25-fold more DEGs for the excitatory neuron subset (Micro2_Exc) compared to the microglial subset (Micro2_Micro), indicating excitatory neurons as the primary source of differential gene expression for this cluster. Biological pathway analysis revealed that the top enriched pathways across cell subtypes included synaptic transmission, neuronal morphology, protein folding, and proteolysis (Figure 6Dii). The strongest enrichment was observed in Micro2 excitatory neurons followed by multiple oligodendrocyte and other excitatory neuron subtypes, as well as Micro2 microglia. Synaptic transmission-associated pathways were most strongly enriched in excitatory neuron subtypes. DLB- and PD-GWAS genes strongly upregulated in DLB were also associated with these functional categories, including synaptic adhesion-related genes *ADAM15* and *GPNMB* in Exc7, and synaptic vesicle-trafficking gene *RUSC1* in Micro2 (Figure 6Di). Chromatin remodeling GWAS genes were DLB-upregulated across multiple clusters, including *ATXN7L3* and *TOX3* in Micro2, *KAT8* in Oligo2, and *SALL1* in Oligo3, while the TF *ELK4* was DLB-upregulated in all three clusters. The DNA repair-associated gene *NUCKS1* and actin gene *ATCB* were highly DLB-upregulated in both oligodendrocyte clusters Oligo2 and 3. Notably, *SNCA* and the amyloid precursor protein (APP)-processing gene *LDLRAD3* were both among the most highly DLB-upregulated GWAS genes in Oligo3.

Di, Venn diagram showing overlap between DEGs downregulated in each NDD within the Interneuron 2 subtype. Dii, Unbiased volcano plots for GABAergic neuron 1 subtype gene expression in each NDD. Log2 fold change (FC) between NDD nuclei and NC nuclei of the same subtype is plotted against −log10 *P* value (FDR). Points representing DEGs with statistically significant (FDR < 0.05) upregulation in NDD are shown in dark red while DEGs with significant downregulation are shown in dark blue. Genes without significantly differential expression are shown as gray points. The three DEGs with the highest absolute fold change (log2FC > 0.2) in the up- and downregulated categories are labeled in dark red and dark blue, respectively. The three DEGs within 500 kb of NDD-associated SNPs previously identified in GWAS (GWAS-DEG) with the highest absolute log2FC in the up- and downregulated categories are labeled in bright red and bright blue, respectively. Basic functional category information is indicated for each labeled GWAS-DEG. Diii, Metascape network plots of biological pathways enriched among DEGs downregulated in all NDDs within the GABAergic neuron 1 subtype. Nodes represent specific biological pathways clustered by shared gene membership. Clusters with similar biological function are color coded and labeled according to general function. Node sizes are proportional to the number of differential-interacting genes in the pathway, and line width connecting nodes is proportional to shared gene membership in linked pathways. Div, Metascape bar chart showing the top 20 most highly enriched biological pathway terms among DEGs downregulated across all NDDs within the GABAergic neuron 1 subtype. Statistical significance (Log10 *P* value) is plotted on horizontal axes. Darker-colored bars indicated greater significance. Ei, Venn diagram showing overlap between DEGs downregulated in each NDD within the GABAergic neuron 1 subtype. Eii, Unbiased volcano plots for Interneuron 2 subtype gene expression in each NDD. Eiii, Metascape network plots of biological pathways enriched among DEGs upregulated in all NDDs within the Interneuron 2 subtype. Eiv, Metascape bar chart showing the top 20 most highly enriched biological pathway terms among DEGs downregulated across all NDDs within the Interneuron 2 subtype. Fi, Venn diagram showing overlap between DEGs upregulated in each NDD within the Microglia 10 subtype. Fii, Unbiased volcano plots for Microglia 10 subtype gene expression in each NDD. Fiii, Metascape network plots of biological pathways enriched among DEGs upregulated in all NDDs within the Microglia 10 subtype. Fiv, Metascape bar chart showing the top 20 most highly enriched biological pathway terms among DEGs upregulated across all NDDs within the Microglia 10 subtype. AD, Alzheimer's disease; DEG, differentially expressed gene; DLB, dementia with Lewy bodies; FDR, false discovery rate; GWAS, genome-wide association study; NC, normal control; NDD, neurodegenerative disease; PD, Parkinson's disease.

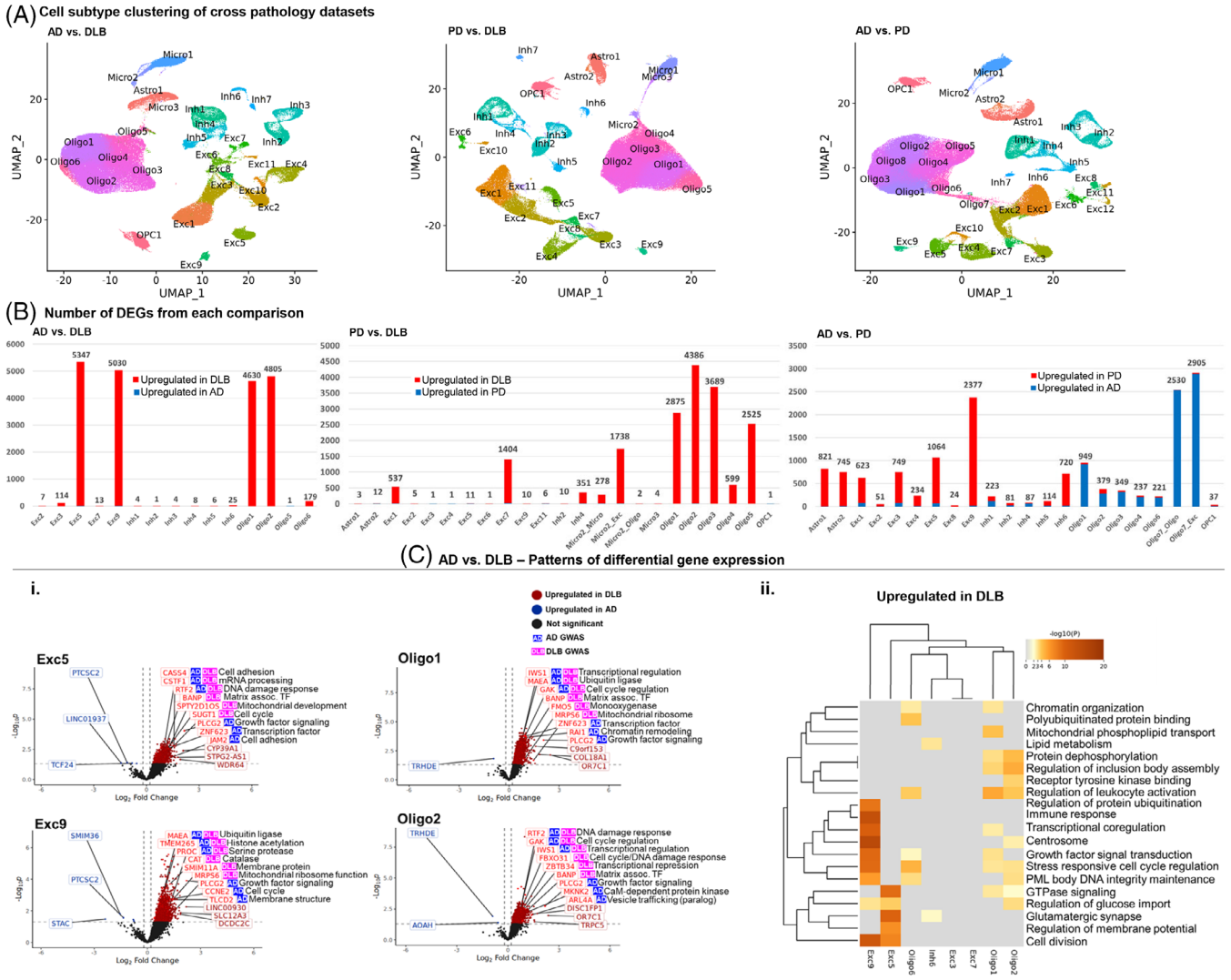

FIGURE 6 Differential gene expression between NDDs in cell subtypes. A, Uniform Manifold Approximation and Projection for Dimension Reduction dimensional reduction plots of integrated pairs of NDD nuclei of all cell types, color coded to indicate cell subtype clusters. B, Bar charts representing numbers of DEGs identified using NEBULA for each cell subtype between nuclei of the indicated NDD pairs within the same subtype. Red and blue bars represent DEGs upregulated in one or the other NDD, as indicated. Ci, Unbiased volcano plots showing gene expression in selected cell subtypes in the AD and DLB comparison. Log2 fold change (FC) between nuclei of the 2 NDDs in the same subtype is plotted against −log10 *P* value (FDR). Points representing DEGs with statistically significant (FDR < 0.05) upregulation in AD are shown in dark blue while DEGs with significant upregulation in DLB are shown in dark red. Genes without significantly differential expression are shown as gray points. The three DEGs with the highest absolute fold change (log2FC > 0.2) in the AD and DLB upregulated categories are labeled in dark blue and dark red, respectively. The three DEGs within 500 kb of NDD-associated single nucleotide polymorphisms previously identified in GWAS (GWAS-DEG) exclusive to AD, exclusive to DLB, and common to both NDDs with the highest absolute log2FC in the up- and downregulated categories are labeled in bright red and bright blue, respectively, and the NDDs associated with each GWAS-DEG are indicated. Basic functional category information is indicated for each labeled GWAS-DEG. Cii, Heatmap of top 20 enriched pathways among interactions increased in DLB compared to AD across all cell types. Color saturation is proportional to statistical significance of enrichment. Di, Unbiased volcano plots showing gene expression in selected cell subtypes in the PD and DLB comparison. Color coding indicates upregulation in the indicated NDD. The top three GWAS-DEGs exclusive to PD, exclusive to DLB, and common to both NDDs are indicated. Dii, Heatmap of top 20 enriched pathways among interactions increased in DLB compared to PD across all cell types. Ei, Unbiased volcano plots showing gene expression in selected cell subtypes in the AD and PD comparison. Color coding indicates upregulation in the indicated NDD. The top three GWAS-DEGs exclusive to AD, exclusive to PD, and common to both NDDs are indicated. Eii, Heatmap of top 20 enriched pathways among interactions increased in PD compared to AD across all cell types. Eiii, Heatmap of top 20 enriched pathways among interactions increased in AD compared to PD across all cell types. AD, Alzheimer's disease; DEG, differentially expressed gene; DLB, dementia with Lewy bodies; FDR, false discovery rate; GWAS, genome-wide association study; NC, normal control; NDD, neurodegenerative disease; PD, Parkinson's disease.

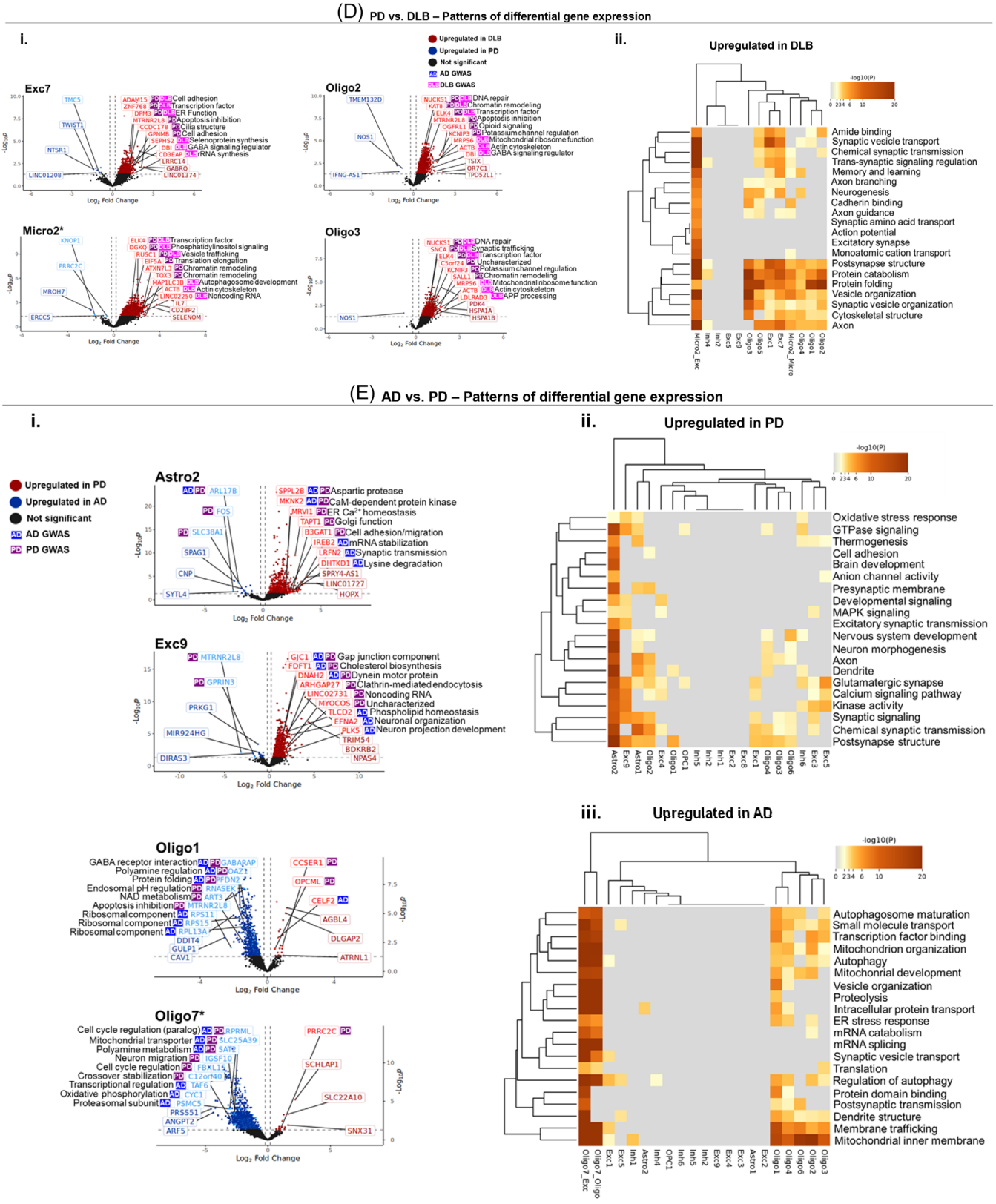

FIGURE 6 Continued

Comparing AD to PD yielded the most diverse pattern of transcriptional dysregulation as demonstrated by the variety of cell types with DEGs and the directionality of the differential expression (Figure 6B, Ei, Tables S23–S27 in supporting information). Upregulation in PD was observed in astrocyte (821 and 745 DEGs in Astro1 and 2, respectively), excitatory (623, 749, 1064, and 2377 in Exc1, 3, 5, and 9, respectively) and inhibitory neuron clusters (720 in Inh6), while upregulation in AD was observed primarily in oligodendrocyte clusters (949 in Oligo1). The largest number of DEGs upregulated in AD was observed in the Oligo7 cluster. However, this subtype represents a hybrid cluster, comprised of similar numbers of nuclei annotated as oligodendrocytes and excitatory neurons (42.4% and 38.4% of cluster nuclei, respectively). Thus, oligodendrocytes (Oligo7_Oligo) and excitatory neurons (Oligo7_Exc) in this cluster were analyzed separately for differential gene expression. Similar numbers of DEGs were identified for each of these subsets (2530 for Oligo7_Oligo and 2905 for Oligo7_Exc).

Biological pathway analysis of the PD-upregulated DEGs for each cell subtype showed the strongest enrichment in the Astro2 subtype, followed by other astrocyte, excitatory neuron, and oligodendrocyte clusters (Figure 6Eii). These were dominated by pathways associated with neuronal morphogenesis/organization and synaptic transmission. Accordingly, the most strongly upregulated AD- and PD-GWAS genes were also involved in cell morphogenesis and organization, including *B3GAT1* in Astro2, and *GJC1*, *EFNA2*, and *PLK5* in Exc9 (Figure 6Ei). Genes upregulated in AD over PD showed the strongest enrichment for pathways in the Oligo7 cluster (both Oligo and Exc subsets) as well as several other oligodendrocyte clusters (Figure 6Eiii). Across these cell types, the top enriched pathways were largely associated with autophagy, mitochondrial structure, membrane trafficking, and mRNA processing. However, in Oligo1 and 7, the most strongly AD-upregulated individual GWAS genes were mainly associated with different pathways, including numerous protein synthesis and maturation-associated DEGs (Figure 6Ei). These included ribosomal genes *RPS11*, *RPS15*, and *RPL13A*, and chaperone *PFDN2* in Oligo1, and genes associated with cell cycle regulation (*FLBXL15*, *RPRML*), proteolysis (*FLBXL15*, *PSMC5*), and mitochondrial oxidative metabolism (*SLC25A39*, *CYC1*) in Oligo7.

To summarize, comparison of gene expression in DLB to either AD or PD primarily revealed gene upregulation in DLB within relatively few excitatory neuron and oligodendrocyte cell subtypes, but comparison of AD to PD revealed more diverse patterns of differential gene expression, with upregulation in PD within astrocyte, excitatory neuron, and inhibitory neuron clusters, and upregulation in AD within numerous oligodendrocyte clusters.

4 | DISCUSSION

Here, we used snRNA-seq datasets obtained from three major NDDs to gain insight into key aspects of pathogenesis, including: (1) vulnerability of specific cell subtypes, (2) disease-driver cell subtypes based on enriched expression of GWAS genes, (3) changes in cell-to-cell communication, and (4) shared and (5) differential gene expression patterns and biological pathways (Figure 1B). As we focused on a neocortical brain region, our findings should advance the understanding of shared and distinct processes contributing to the neuropathological propagation and associated progression of clinical symptoms across these NDDs.

While vulnerable neuronal populations have been described for individual NDDs,[62–64] no previous work has directly compared vulnerability of the same cell subtypes across NDDs. We found that AD and DLB share a common vulnerable inhibitory neuron subtype characterized by expression of the interneuron marker *VIP* and inhibition of *PVALB*, *SST*, and *HTR3A*. Previous work demonstrated VIP^+ interneurons to moderate cortical disinhibitory circuits, inhibiting $PVALB^+$ and SST^+ interneurons and thereby preventing inhibition of pyramidal neurons, thus regulating motor integration and cortical plasticity.[65] Loss of this subtype may suggest involvement in symptoms common to both AD and DLB. In PD, previous work has focused on vulnerable cell types within the SN.[63] Here, we identified an inhibitory neuron cluster depleted within the TC distinct from depleted populations in AD and DLB. This suggests potential association of this cell type with PD-specific cortical disease progression and pathology,[66–69] but more direct evidence is required to support such an assertion.

To better understand brain cell types driving disease risk in NDDs, we examined enrichment of gene expression within GWAS regions. Multiple cortical neuronal subtypes were implicated as disease drivers in PD and DLB. The severity of cognitive impairment in Lewy body dementias is correlated with cortical Lewy body accumulation,[70] particularly within the temporal lobe compared to frontal or limbic cortical regions.[35] Furthermore, cortical neurotransmitter dysregulation and synaptic dysfunction likely play a central role in cognitive impairment in both PD[71–74] and DLB.[75,76] Consistently, we found that disease-driving neurons for DLB and PD were primarily excitatory subtypes, and the enriched GWAS genes showing differential expression were largely associated with synaptic function.

In AD, we predicted only a single disease-driving oligodendrocyte population. While studies have focused mainly on disease-associated microglia in AD pathogenesis,[77–79] the involvement of oligodendrocytes is also evident.[80,81] Demyelination often precedes neuronal loss in AD,[82] causing neurodegeneration through disruption of metabolic axon support and maintenance.[83] Oligodendrocyte-mediated myelin loss may thus represent a primary feature of AD pathology.[84] The importance of AD risk gene expression in oligodendrocytes has also been established.[85] For example, the major AD risk-associated gene *BIN1*, involved in vesicle endocytosis and apoptosis, is primarily expressed in oligodendrocytes and has been implicated in AD-associated demyelination.[86] We identified *BIN1* inhibition in the disease-driver oligodendrocyte cluster of AD nuclei, along with increased expression of numerous other AD-GWAS genes associated with vesicle trafficking and apoptosis, including *PICALM* and *SNX1*. Dysregulation of these processes within disease-driver oligodendrocytes may contribute to oligodendrocyte dysfunction and AD progression within the TC.

Analysis of altered cell-to-cell communication also highlighted oligodendrocyte subtypes in all three NDDs, in addition to several neuronal subtypes. While in AD the strength of many communication pathways was increased, overall decreased communication was observed in DLB and PD. Together with our identification of the disease-driver cell types, these changes in cellular communication suggest an increased involvement of oligodendrocyte–neuron interaction in AD, while communication between and within these cell types may be inhibited in the context of the synucleopathies. Dysregulation of oligodendrocyte–neuron interactions would presumably lead to aberrant myelination resulting in neuronal dysfunction and loss.

We also studied shared dysregulation of gene expression across NDDs, and identified the most shared DEGs among inhibitory neurons. Previous studies have established an important role for inhibitory neurons in AD,[87,88] demonstrating that GABAergic neurotransmission is impaired both in humans[89–92] and murine AD models,[93–95] leading to hyperexcitability of neural circuits and likely contributing to cognitive dysfunction. In PD, dysregulation of GABAergic neurotransmission is likely a primary driver of motor deterioration.[96] Overaccumulation of intracellular Ca^{2+} along with *SNCA* is directly associated with neuronal death in PD in part through mitochondrial-stress-induced apoptosis,[97,98] while GABA signaling prevents Ca^{2+} influx, thereby protecting neurons from calcium toxicity.[98] Loss of dopaminergic neurons in the SN is furthermore predicted to dysregulate GABAergic neurotransmission.[99,100] These findings support the importance of inhibitory neurons in both cognitive decline in AD and motor deterioration in PD, and potentially in the combination of these symptoms in DLB. Furthermore, our pathway analysis in inhibitory neuron subtypes revealed dysregulation of numerous genes involved in mitochondrial processes across the NDDs, possibly indicating altered metabolic activity due to neurological dysfunction.

We investigated disease-specific molecular determinants by direct comparison of differential gene expression between pathologies and found that a relatively small number of cell subtypes displayed strong differential gene expression in DLB compared to either AD or PD, with almost all DEGs upregulated in DLB. In contrast, comparing AD versus PD, most cell subtypes exhibited relatively high numbers of DEGs, with greater diversity in the directionality of differential expression across cell types. This indicates overall greater transcriptomic overlap between DLB and the other two NDDs, while AD and PD show more divergence. These results provide molecular support to the paradigm wherein DLB is "intermediate" on the continuum of AD–PD spectrum disorders, consistent with the clinical manifestations of the NDDs, wherein both AD and DLB are defined by pronounced dementia,[7,101] while PD and DLB both share motor deterioration as a clinical hallmark.[7,102] On the other hand, motor symptoms are not typically associated with AD,[101] and PD is commonly associated with mild or absent cognitive decline, specifically in the early disease stages.[67]

In all cross-NDD comparisons, we identified DEGs predominantly in excitatory neurons and oligodendrocytes. Comparisons of PD to both AD and DLB identified multiple oligodendrocyte clusters with altered transcriptional profiles. Consistently, previous single-cell sequencing studies have revealed enriched expression of PD-GWAS genes in oligodendrocytes of the SN,[103] as well as depletion of midbrain oligodendrocytes in PD patients.[104] Furthermore, PD-specific oligodendrocyte populations have been predicted to display aberrant myelination activity.[105] Together with these previous findings, our data suggest an important role for oligodendrocytes in PD that is distinct from both AD and DLB.

This work provides an essential direct comparison of the molecular underpinnings of three major NDDs. However, there are some limitations. First, for direct comparison, it was necessary to examine the same brain region in each NDD. However, regions are affected differently in each condition. To overcome this limitation, we selected the TC for analysis, a region impacted in all three diseases.[35,38,106–111] As the TC is generally affected in later stages of disease progression for PD than for AD and DLB,[40] our data for PD reflect transcriptional changes preliminary to major cortical neurodegeneration and provide insight into the molecular basis for PD progression into this region. Future studies comparing single-cell transcriptional profiles of cortical samples from different stages of PD would be invaluable in better understanding the molecular changes associated with PD progression and cognitive decline. Second, while we have taken numerous measures to control for potential confounding effects of sample variation, including but not limited to rigorous QC filtering, covariate selection and regression, and inclusion of sample ID as a random effect in our differential expression modeling, in studies using human-archived brain tissues, it is a challenge to build a unified cohort and to perfectly control for all such confounding variability. Third, to control for potential transcriptomic effects of *APOE*, we constrained the analysis to donors with the *APOE* $\varepsilon3/\varepsilon3$ genotype. Differences in the transcriptomic profiles between patient carriers of the $\varepsilon3$ and $\varepsilon4$ alleles warrant further investigation in future work. Last, we would like to reiterate the caveat that in this work we inferred and interpreted the relationships between gene expression patterns and pathogenic mechanisms based on our transcriptomic observations. Future empirical experimentation using human-induced polypotent stem cell and rodent model systems of NDDs is necessary as the next step to validate the findings of key cell types, genes, and cell–cell communication pathways.

It should be noted that each of these NDD categories represent a complex range of comorbid clinical symptoms and co-pathologies. Four major subtypes of AD have been characterized based on pathological factors,[112] while another study identified five molecular subtypes using cerebrospinal fluid proteomics.[113] Likewise, PD has been divided into three distinct subtypes based on both motor and non-motor factors.[114] DLB is particularly complex to define due to its shared clinical features with both AD and PD, but specific subtypes of this disease have also been described based on patterns of α-synuclein and tau distribution.[115] Future studies may aim to elucidate the transcriptomic mechanisms underlying these pathological subtypes to develop an even higher-resolution understanding of the specific genetic factors driving diverse clinical outcomes. Because of this heterogeneity, there is no single "silver bullet" for fighting neurodegeneration, but our findings contribute to a framework for the development of

targeted treatment strategies tailored to the specific clinical challenges presented by each of these important diseases.

ACKNOWLEDGMENTS

The authors thank the Kathleen Price Bryan Brain Bank at Duke University (funded by NIH/NIA R01 AG028377) for providing us with the brain tissues, and the Duke Sequencing and Genomic Technologies Shared Resource for sequencing. This study used a high-performance computing facility partially supported by grant 2016-IDG-1013 ("HARDAC+: Reproducible HPC for Next-generation Genomics") from the North Carolina Biotechnology Center. This work was funded in part by the National Institute of Neurological Disorders & Stroke (NINDS/NIH; RF1-NS113548-01A1 to OC-F) and by the National Institutes of Health/National Institute on Aging (NIH/NIA; R01 AG057522 and RF1 AG077695 to OC-F). We are grateful to the Banner Sun Health Research Institute Brain and Body Donation Program of Sun City, Arizona for the provision of human biological materials. The Brain and Body Donation Program has been supported by the National Institute of Neurological Disorders and Stroke (U24 NS072026 National Brain and Tissue Resource for Parkinson's Disease and Related Disorders), the National Institute on Aging (P30 AG019610 and P30AG072980, Arizona Alzheimer's Disease Center), the Arizona Department of Health Services (contract 211002, Arizona Alzheimer's Research Center), the Arizona Biomedical Research Commission (contracts 4001, 0011, 05-901, and 1001 to the Arizona Parkinson's Disease Consortium), and the Michael J. Fox Foundation for Parkinson's Research. This work is dedicated to Olivia Louise Shwab.

CONFLICT OF INTEREST STATEMENT

None. Author disclosures are available in the supporting information.

ETHICS STATEMENT

The project was approved by the Duke Institutional Review Board. The study does not involve living human subjects. All samples were obtained from autopsies, and all are de-identified.

ORCID

E. Keats Shwab https://orcid.org/0000-0002-8383-1031
Zhaohui Man https://orcid.org/0000-0003-2537-1425
Daniel C. Gingerich https://orcid.org/0009-0008-9886-9391
Julia Gamache https://orcid.org/0000-0002-3750-147X
Melanie E. Garrett https://orcid.org/0000-0003-2302-6150
Geidy E. Serrano https://orcid.org/0000-0002-9527-2011
Thomas G. Beach https://orcid.org/0000-0003-3296-6128
Gregory E. Crawford https://orcid.org/0000-0001-6106-2772
Allison E. Ashley-Koch https://orcid.org/0000-0001-5409-9155
Ornit Chiba-Falek https://orcid.org/0000-0002-2529-8785

REFERENCES

1. Hamilton R. Lewy bodies in Alzheimer's disease: a neuropathological review of 145 cases using alpha-synuclein immunohistochemistry. *Brain Pathol*. 2000;10:378-384.
2. Twohig D, Nielsen H. α-synuclein in the pathophysiology of Alzheimer's disease. *Mol Neurodegener*. 2019;14:23.
3. Kotzbauer P, Giasson BI, Kravitz AV, et al. Fibrillization of alpha-synuclein and tau in familial Parkinson's disease caused by the A53T alpha-synuclein mutation. *Exp Neurol*. 2004;187:279-288.
4. Ishizawa T, Mattila P, Davies P, Wang D, Dickson D. Colocalization of tau and alpha-synuclein epitopes in Lewy bodies. *J Neuropathol Exp Neurol*. 2003;62:389-397.
5. Arima K, Mizutani T, Alim MA, et al. NACP/alpha-synuclein and tau constitute two distinctive subsets of filaments in the same neuronal inclusions in brains from a family of parkinsonism and dementia with Lewy bodies: double-immunolabeling fluorescence and electron microscopic studies. *Acta Neuropathol*. 2000;100:115-121.
6. Coughlin D, Hurtig H, Irwin D. Pathological influences on clinical heterogeneity in Lewy body diseases. *Mov Disord*. 2020;35:5-19.
7. McKeith IG, Boeve BF, Dickson DW, et al. Diagnosis and management of dementia with Lewy bodies: fourth consensus report of the DLB Consortium. *Neurology*. 2017;89:88-100.
8. Meeus B, Theuns J, Van Broeckhoven C. The genetics of dementia with Lewy bodies: what are we missing?. *Arch Neurol*. 2012;69:1113-1118.
9. Sengupta U, Kayed R. Amyloid β, Tau, and α-Synuclein aggregates in the pathogenesis, prognosis, and therapeutics for neurodegenerative diseases. *Prog Neurobiol*. 2022;214:102270.
10. Kunkle BW, Grenier-Boley B, Sims R, et al. Genetic meta-analysis of diagnosed Alzheimer's disease identifies new risk loci and implicates Abeta, tau, immunity and lipid processing. *Nat Genet*. 2019;51:414-430.
11. Bellenguez C, Küçükali F, Jansen IE, et al. New insights into the genetic etiology of Alzheimer's disease and related dementias. *Nat Genet*. 2022;54:412-436. doi:10.1038/s41588-022-01024-z
12. Kunkle BW, Schmidt M, Klein H, et al. Novel Alzheimer disease risk loci and pathways in African American individuals using the African Genome Resources Panel: a meta-analysis. *JAMA Neurol*. 2021;78:102-113.
13. Nalls MA, Blauwendraat C, Vallerga CL, et al. Identification of novel risk loci, causal insights, and heritable risk for Parkinson's disease: a meta-analysis of genome-wide association studies. *Lancet Neurol*. 2019;18:1091-1102.
14. Kim JJ, Vitale D, Otani DV, et al. Multi-ancestry genome-wide association meta-analysis of Parkinson's disease. *Nat Genet*. 2024;56:27-36.
15. Guerreiro R, Ross OA, Kun-Rodrigues C, et al. Investigating the genetic architecture of dementia with Lewy bodies: a two-stage genome-wide association study. *Lancet Neurol*. 2018;17:64-74.
16. Chia R, Sabir MS, Bandres-Ciga S, et al. Genome sequencing analysis identifies new loci associated with Lewy body dementia and provides insights into its genetic architecture. *Nat Genet*. 2021;53:294-303.
17. Szwedo AA, Dalen I, Pedersen KF, et al. GBA and APOE impact cognitive decline in Parkinson's disease: a 10-year population-based study. *Mov Disord*. 2022;37:1016-1027.
18. Wang Q, Tian Q, Song X, Liu Y, Li W. SNCA gene polymorphism may contribute to an increased risk of Alzheimer's disease. *J Clin Lab Anal*. 2016;30:1092-1099.
19. Meeus B, Verstraeten A, Crosiers D, et al. DLB and PDD: a role for mutations in dementia and Parkinson disease genes?. *Neurobiol Aging*. 2012;33:629.e5-629.e18.
20. Ishikawa A, Piao Y, Miyashita A, et al. A mutant PSEN1 causes dementia with Lewy bodies and variant Alzheimer's disease. *Ann Neurol*. 2005;57:429-434.
21. Leverenz JB, Fishel MA, Peskind ER, et al. Lewy body pathology in familial Alzheimer disease: evidence for disease- and mutation-specific pathologic phenotype. *Arch Neurol*. 2006;63:370-376.
22. Zimprich A, Müller-Myhsok B, Farrer M, et al. The PARK8 locus in autosomal dominant parkinsonism: confirmation of linkage and

further delineation of the disease-containing interval. *Am J Hum Genet*. 2004;74:11-19.
23. Colom-Cadena M, Gelpi E, Martí MJ, et al. MAPT H1 haplotype is associated with enhanced α-synuclein deposition in dementia with Lewy bodies. *Neurobiol Aging*. 2013;34:936-942.
24. Bras J, Guerreiro R, Darwent L, et al. Genetic analysis implicates APOE, SNCA and suggests lysosomal dysfunction in the etiology of dementia with Lewy bodies. *Hum Mol Genet*. 2014;23:6139-6146.
25. Mathys H, Davila-Velderrain J, Peng Z, et al. Single-cell transcriptomic analysis of Alzheimer's disease. *Nature*. 2019;570:332-337.
26. Morabito S, Miyoshi E, Michael N, et al. Single-nucleus chromatin accessibility and transcriptomic characterization of Alzheimer's disease. *Nat Genet*. 2021;53:1143-1155.
27. Anderson AG, Rogers BB, Loupe JM, et al. Single nucleus multiomics identifies ZEB1 and MAFB as candidate regulators of Alzheimer's disease-specific cis-regulatory elements. *Cell Genom*. 2023;3:100263.
28. Gamache J, Gingerich D, Shwab EK, et al. Integrative single-nucleus multi-omics analysis prioritizes candidate cis and trans regulatory networks and their target genes in Alzheimer's disease brains. *Cell Biosci*. 2023;13:185.
29. Kamath T, Abdulraouf A, Burris SJ, et al. Single-cell genomic profiling of human dopamine neurons identifies a population that selectively degenerates in Parkinson's disease. *Nature Neurosci*. 2022;25:588-595.
30. Lee AJ, Kim C, Park S, et al. Characterization of altered molecular mechanisms in Parkinson's disease through cell type-resolved multiomics analyses. *Sci Adv*. 2023;9:eabo2467.
31. Rajkumar AP, Bidkhori G, Shoaie S, et al. Postmortem cortical transcriptomics of Lewy body dementia reveal mitochondrial dysfunction and lack of neuroinflammation. *Am J Geriatr Psychiatry*. 2020;28:75-86.
32. Pietrzak M, Papp A, Curtis A, et al. Gene expression profiling of brain samples from patients with Lewy body dementia. *Biochem Biophys Res Commun*. 2016;479:875-880.
33. Santpere G, Garcia-Esparcia P, Andres-Benito P, et al. Transcriptional network analysis in frontal cortex in Lewy body diseases with focus on dementia with Lewy bodies. *Brain Pathol*. 2018;28:315-333.
34. Lam B, Masellis M, Freedman M, Stuss D, Black S. Clinical, imaging, and pathological heterogeneity of the Alzheimer's disease syndrome. *Alzheimers Res Ther*. 2013;5:1.
35. Harding A, Halliday G. Cortical Lewy body pathology in the diagnosis of dementia. *Acta Neuropathol*. 2001;102:355-363.
36. Aarsland D, Perry R, Brown A, Larsen J, Ballard C. Neuropathology of dementia in Parkinson's disease: a prospective, community-based study. *Ann Neurol*. 2005;58:773-776.
37. Lippa CF, Duda JE, Grossman M, et al. DLB and PDD boundary issues: diagnosis, treatment, molecular pathology, and biomarkers. *Neurology*. 2007;68:812-819.
38. Dubois B, Feldman HH, Jacova C, et al. Research criteria for the diagnosis of Alzheimer's disease: revising the NINCDS-ADRDA criteria. *Lancet Neurol*. 2007;6:734-746.
39. Beach TG, Adler CH, Sue LI, et al. Arizona study of aging and neurodegenerative disorders and brain and body donation program. *Neuropathology*. 2015;35:354-389.
40. McKeith IG, Dickson DW, Lowe J, et al. Diagnosis and management of dementia with Lewy bodies: third report of the DLB Consortium. *Neurology*. 2005;65:1863-1872.
41. Adler CH, Beach TG, Zhang N, et al. Unified staging system for Lewy body disorders: clinicopathologic correlations and comparison to Braak Staging. *J Neuropathol Exp Neurol*. 2019;78:891-899.
42. Jiang Y, Matevossian A, Huang H, Straubhaar J, Akbarian S. Isolation of neuronal chromatin from brain tissue. *BMC Neurosci*. 2008;9:42.
43. Marzluff W. Preparation of active nuclei. *Methods Enzymol*. 1990;181:30-36.
44. Hao Y, et al. Integrated analysis of multimodal single-cell data. *bioRxiv*. 2020. 2020.10.12.335331.
45. Hafemeister C, Satija R. Normalization and variance stabilization of single-cell RNA-seq data using regularized negative binomial regression. *Genome Biol*. 2019;20:296.
46. Lause J, Berens P, Kobak D. Analytic Pearson residuals for normalization of single-cell RNA-seq UMI data. *bioRxiv*. 2020. 2020.12.01.405886.
47. Stuart T, Butler A, Hoffman P, et al. Comprehensive integration of single-cell data. *Cell*. 2019;177:1888-1902 e21.
48. Grubman A, Chew G, Ouyang JF, et al. A single-cell atlas of entorhinal cortex from individuals with Alzheimer's disease reveals cell-type-specific gene expression regulation. *Nat Neurosci*. 2019;22:2087-2097.
49. Yang L, Ng YE, Sun H, et al. Single-cell Mayo Map (scMayoMap): an easy-to-use tool for cell type annotation in single-cell RNA-sequencing data analysis. *BMC Biol*. 2023;21:223.
50. Bakken T, et al. Evolution of cellular diversity in primary motor cortex of human, marmoset monkey, and mouse. *bioRxiv*. 2020. 2020.03.31.016972.
51. He L, Davila-Velderrain J, Sumida TS, Hafler DA, Kellis M, Kulminski AM. NEBULA is a fast negative binomial mixed model for differential or co-expression analysis of large-scale multi-subject single-cell data. *Commun Biol*. 2021;4:629.
52. Gagnon J, Pi L, Ryals M, et al. Recommendations of scRNA-seq differential gene expression analysis based on comprehensive benchmarking. *Life (Basel)*. 2022;12:850.
53. Jin S, Guerrero-Juarez CF, Zhang L, et al. Inference and analysis of cell-cell communication using CellChat. *Nat Commun*. 2021;12:1088.
54. Zhou Y, Zhou B, Pache L, et al. Metascape provides a biologist-oriented resource for the analysis of systems-level datasets. *Nat Commun*. 2019;10:1523.
55. Bakken TE, Jorstad NL, Hu Q, et al. Comparative cellular analysis of motor cortex in human, marmoset and mouse. *Nature*. 2021;598:111-119.
56. Wei J, Hao Z, Xu C, et al. Identification of visual cortex cell types and species differences using single-cell RNA sequencing. *Nat Commun*. 2022;13:6902.
57. Lake BB, Chen S, Sos BC, et al. Integrative single-cell analysis of transcriptional and epigenetic states in the human adult brain. *Nat Biotechnol*. 2018;36:70-80.
58. Hodge RD, Bakken TE, Miller JA, et al. Conserved cell types with divergent features in human versus mouse cortex. *Nature*. 2019;573:61-68.
59. Marinaro F, et al. Molecular and cellular pathology of monogenic Alzheimer's disease at single cell resolution. *bioRxiv*. 2020. 2020.07.14.202317.
60. Gazestani V, Kamath T, Nadaf NM, et al. Early Alzheimer's disease pathology in human cortex involves transient cell states. *Cell*. 2023;186:4438-4453.e23.
61. Aibar S, González-Blas CB, Moerman T, et al. SCENIC: single-cell regulatory network inference and clustering. *Nature Methods*. 2017;14:1083-1086.
62. Mrdjen D, Fox EJ, Bukhari SA, Montine KS, Bendall SC, Montine TJ. The basis of cellular and regional vulnerability in Alzheimer's disease. *Acta Neuropathol*. 2019;138:729-749.
63. Giguère N, Burke Nanni S, Trudeau L. On cell loss and selective vulnerability of neuronal populations in Parkinson's disease. *Front Neurol*. 2018;9:455.
64. Harraz M. Selective dopaminergic vulnerability in Parkinson's disease: new insights into the role of DAT. *Front Neurosci*. 2023;17:1219441.
65. Georgiou C, Kehayas V, Lee KS, et al. A subpopulation of cortical VIP-expressing interneurons with highly dynamic spines. *Communications Biology*. 2022;5:352.

66. Foltynie T, Brayne C, Robbins T, Barker R. The cognitive ability of an incident cohort of Parkinson's patients in the UK. The CamPaIGN study. *Brain*. 2004;127:550-560.
67. Aarsland D, Batzu L, Halliday GM, et al. Parkinson disease-associated cognitive impairment. *Nat Rev Dis Primers*. 2021;7:47.
68. Aarsland D, Brønnick K, Larsen J, Tysnes O, Alves G. Cognitive impairment in incident, untreated Parkinson disease: the Norwegian ParkWest study. *Neurology*. 2009;72:1121-1126.
69. Elgh E, Domellöf M, Linder J, Edström M, Stenlund H, Forsgren L. Cognitive function in early Parkinson's disease: a population-based study. *Eur J Neurol*. 2009;16:1278-1284.
70. Mattila PM, Rinne JO, Helenius H, Dickson DW, Röyttä M, Mattila PM. Alpha-synuclein-immunoreactive cortical Lewy bodies are associated with cognitive impairment in Parkinson's disease. *Acta Neuropathol*. 2000;100:285-290.
71. Pagonabarraga J, Kulisevsky J. Cognitive impairment and dementia in Parkinson's disease. *Neurobiol Dis*. 2012;46:590-596.
72. Narayanan N, Rodnitzky R, Uc E. Prefrontal dopamine signaling and cognitive symptoms of Parkinson's disease. *Rev Neurosci*. 2013;24:267-278.
73. Kehagia A, Barker R, Robbins T. Neuropsychological and clinical heterogeneity of cognitive impairment and dementia in patients with Parkinson's disease. *Lancet Neurol*. 2010;9:1200-1213.
74. Halliday G, Leverenz J, Schneider J, Adler C. The neurobiological basis of cognitive impairment in Parkinson's disease. *Mov Disord*. 2014;29:634-650.
75. McKeith I. Dementia with Lewy bodies. *Handb Clin Neurol*. 2007;84:531-548.
76. Schulz-Schaeffer W. The synaptic pathology of alpha-synuclein aggregation in dementia with Lewy bodies, Parkinson's disease and Parkinson's disease dementia. *Acta Neuropathol*. 2010;120:131-143.
77. Deczkowska A, Keren-Shaul H, Weiner A, Colonna M, Schwartz M, Amit I. Disease-associated microglia: a universal immune sensor of neurodegeneration. *Cell*. 2018;173:1073-1081.
78. Wang C, Zong S, Cui X, et al. The effects of microglia-associated neuroinflammation on Alzheimer's disease. *Front Immunol*. 2023;14:1117172.
79. Hansen D, Hanson J, Sheng M. Microglia in Alzheimer's disease. *J Cell Biol*. 2018;217:459-472.
80. Butt A, De La Rocha I, Rivera A. Oligodendroglial cells in Alzheimer's disease. *Adv Exp Med Biol*. 2019;1175:325-333.
81. Wang J, Zhen Y, Yang J, Yang S, Zhu G. Recognizing Alzheimer's disease from perspective of oligodendrocytes: phenomena or pathogenesis?. *CNS Neurosci Ther*. 2024;30:e14688.
82. Bartzokis G. Alzheimer's disease as homeostatic responses to age-related myelin breakdown. *Neurobiol Aging*. 2011;32:1341-1371.
83. Stassart R, Möbius W, Nave K, Edgar J. The axon-myelin unit in development and degenerative disease. *Front Neurosci*. 2018;12:467.
84. Nasrabady S, Rizvi B, Goldman J, Brickman A. White matter changes in Alzheimer's disease: a focus on myelin and oligodendrocytes. *Acta Neuropathol Commun*. 2018;6:22.
85. McKenzie AT, Moyon S, Wang M, et al. Multiscale network modeling of oligodendrocytes reveals molecular components of myelin dysregulation in Alzheimer's disease. *Mol Neurodegen*. 2017;12:82.
86. De Rossi P, Buggia-Prévot V, Clayton BLL, et al. Predominant expression of Alzheimer's disease-associated BIN1 in mature oligodendrocytes and localization to white matter tracts. *Mol Neurodegen*. 2016;11:59.
87. Najm R, Jones E, Huang Y. Apolipoprotein E4, inhibitory network dysfunction, and Alzheimer's disease. *Mol Neurodegen*. 2019;14:24.
88. Jiménez-Balado J, Eich T. GABAergic dysfunction, neural network hyperactivity and memory impairments in human aging and Alzheimer's disease. *Semin Cell Dev Biol*. 2021;116:146-159.
89. Bareggi SR. Decreased CSF concentrations of homovanillic acid and gamma-aminobutyric acid in Alzheimer's disease. Age- or disease-related modifications?. *Arch Neurol*. 1982;39:709-712.
90. Gueli M, Taibi G. Alzheimer's disease: amino acid levels and brain metabolic status. *Neurol Sci*. 2013;34:1575-1579.
91. Ramos-Miguel A, Hercher C, Beasley CL, et al. Loss of Munc18-1 long splice variant in GABAergic terminals is associated with cognitive decline and increased risk of dementia in a community sample. *Mol Neurodegen*. 2015;10:65.
92. Li Y, Sun H, Chen Z, Xu H, Bu G, Zheng H. Implications of GABAergic neurotransmission in Alzheimer's disease. *Front Aging Neurosci*. 2016;8:31.
93. Levenga J, Krishnamurthy P, Rajamohamedsait H, et al. Tau pathology induces loss of GABAergic interneurons leading to altered synaptic plasticity and behavioral impairments. *Acta Neuropathol Commun*. 2013;1:34.
94. Ramos B, Baglietto-Vargas D, Rio JCD, et al. Early neuropathology of somatostatin/NPY GABAergic cells in the hippocampus of a PS1×APP transgenic model of Alzheimer's disease. *Neurobiol Aging*. 2006;27:1658-1672.
95. Gold NB, Li D, Chassevent A, et al. Heterozygous de novo variants in CSNK1G1 are associated with syndromic developmental delay and autism spectrum disorder. *Clin Genet*. 2020;98:571-576.
96. Błaszczyk J. Parkinson's disease and neurodegeneration: gABA-Collapse hypothesis. *Front Neurosci*. 2016;10:269.
97. Surmeier D, Schumacker P. Calcium, bioenergetics, and neuronal vulnerability in Parkinson's disease. *J Biol Chem*. 2013;288:10736-10741.
98. Mosharov EV, Larsen KE, Kanter E, et al. Interplay between cytosolic dopamine, calcium, and alpha-synuclein causes selective death of substantia nigra neurons. *Neuron*. 2009;62:218-229.
99. Wang Y, Zhang QJ, Liu J, et al. Changes in firing rate and pattern of GABAergic neurons in subregions of the substantia nigra pars reticulata in rat models of Parkinson's disease. *Brain Res*. 2010;1324:54-63.
100. Faynveitz A, Lavian H, Jacob A, Korngreen A. Proliferation of inhibitory input to the substantia nigra in experimental Parkinsonism. *Front Cell Neurosci*. 2019;13:417.
101. Dubois B, Villain N, Frisoni GB, et al. Clinical diagnosis of Alzheimer's disease: recommendations of the International Working Group. *Lancet Neurol*. 2021;20:484-496.
102. Jankovic J. Parkinson's disease: clinical features and diagnosis. *J Neurol Neurosurg Psychiatry*. 2008;79:368-376.
103. Agarwal D, Sandor C, Volpato V, et al. A single-cell atlas of the human substantia nigra reveals cell-specific pathways associated with neurological disorders. *Nat Commun*. 2020;11:4183.
104. Smajić S, Prada-Medina CA, Landoulsi Z, et al. Single-cell sequencing of human midbrain reveals glial activation and a Parkinson-specific neuronal state. *Brain*. 2022;145:964-978.
105. Bae E, Pérez-Acuña D, Rhee K, Lee S. Changes in oligodendroglial subpopulations in Parkinson's disease. *Mol Brain*. 2023;16:65.
106. Irwin D, Lee V, Trojanowski J. Parkinson's disease dementia: convergence of α-synuclein, tau and amyloid-β pathologies. *Nat Rev Neurosci*. 2013;14:626-636.
107. Sasikumar S, Strafella A. Imaging mild cognitive impairment and dementia in Parkinson's disease. *Front Neurol*. 2020;11:47.
108. Hall H, Reyes S, Landeck N, et al. Hippocampal Lewy pathology and cholinergic dysfunction are associated with dementia in Parkinson's disease. *Brain*. 2014;137:2493-2508.
109. Yu L, Wang T, Wilson RS, et al. Common age-related neuropathologies and yearly variability in cognition. *Ann Clin Transl Neurol*. 2019;6:2140-2149.
110. Smith C, Malek N, Grosset K, Cullen B, Gentleman S, Grosset DG. Neuropathology of dementia in patients with Parkinson's disease: a systematic review of autopsy studies. *J Neurol Neurosurg Psychiatry*. 2019;90:1234-1243.

111. Compta Y, Parkkinen L, O'Sullivan SS, et al. Lewy- and Alzheimer-type pathologies in Parkinson's disease dementia: which is more important?. *Brain*. 2011;134:1493-1505.
112. Ferreira D, Nordberg A, Westman E. Biological subtypes of Alzheimer disease: a systematic review and meta-analysis. *Neurology*. 2020;94:436-448.
113. Tijms BM, Vromen EM, Mjaavatten O, et al. Cerebrospinal fluid proteomics in patients with Alzheimer's disease reveals five molecular subtypes with distinct genetic risk profiles. *Nat Aging*. 2024;4:33-47.
114. Fereshtehnejad S, Zeighami Y, Dagher A, Postuma R. Clinical criteria for subtyping Parkinson's disease: biomarkers and longitudinal progression. *Brain*. 2017;140:1959-1976.
115. Ferman TJ, Aoki N, Boeve BF, et al. Subtypes of dementia with Lewy bodies are associated with α-synuclein and tau distribution. *Neurology*. 2020;95:e155-e165.

SUPPORTING INFORMATION

Additional supporting information can be found online in the Supporting Information section at the end of this article.

How to cite this article: Shwab EK, Man Z, Gingerich DC, et al. Comparative mapping of single-cell transcriptomic landscapes in neurodegenerative diseases. *Alzheimer's Dement*. 2025;21:e70012. https://doi.org/10.1002/alz.70012